NUMERICAL APPROACH TO EVOLUTION EQUATIONS FOR GENERALIZED PARTON DISTRIBUTIONS

Sorawich Maichum

Nan, Thailand

Bachelor of Science, Chiang Mai University, 2019

A Thesis submitted to the Graduate Faculty

of the University of Virginia in Candidacy for the Degree of

Master of Science

Department of Physics

University of Virginia

December 2022

Advisor S. Liuti, Chair

Second M. Vucelja

Numerical approach to Evolution equations for Generalized Parton Distributions

Sorawich Maichum

(ABSTRACT)

We present a numerical code in Python to calculate the evolution equation in perturbative Quantum Chromodynamics (PQCD) for both the parton distributions which are obtained in inclusive deep inelastic scattering experiments, and the generalized parton distributions which can be extracted from deeply virtual exclusive experiments. To solve the integro-differential equations, we adopt the Adams method as an alternative technique to the standard Runge-Kutta algorithm. We compare the relative efficiency of various algorithms for solving the PQCD evolution calculation. The methods are: backward difference, Adams and Runge-Kutta (RK4) We found that the Adams method is the most efficient one in that it decreases the calculation time about four times compared to RK4, while leaving the calculational error about the same.These studies provide an initial step to calculate GPDs evolution.

Dedication

Dedicated to my life and my passion

Acknowledgments

There are many people I am extremely appreciated and I would like to thank for their loves, supports and guidances during the two and a half years of my Physics Master studies. I could not complete my degree and pass the difficult time in my life without their helps.

First of All, I would like to thank for Professor Simonetta Liuti who is my advisor and a chair of the committees. She is a very open -minded, patient and supportive advisor. She always support and advise me while I was on a first dive to develop my instinct into this field which I had never done before. I felt so confused ,frustrated and hopeless at that time. As a result, I can pass the worst time and refine myself into Nuclear Physics slowly with her supports and advice. In addition, I was very appreciated in her understanding, time spending, editing and suggesting on my thesis writing process. After I had a bad time during my master, my academic performances including English skill are worse than I was.

Next one, I would like to thank my parents Sumrith and Punnapa Maichum as well as my partner Luxsanaree Mala for mental supports and others which they can do to hold me passing the struggling time. They always there for me listen, encourage and believe in me whether I did not even believe in myself. They is the main reason that I can keep doing my academic path until I can achieve it.

I would like to thank Jirayu Mongkolkiattichai who is likely my friend and brother for me. He took very good care of me when I am in Charlottesville. Unbelievable that we know each other since we are in the same high school, university and also the former laboratory group for my undergraduate. I am super appreciated and hope he

would achieve his PhD and other achievements untroubledly.

I would like to thank Brandon Kriesten who guided me in an important part of my thesis. When I was confused and frustrated about my research, I cannot find any answers anywhere. I decide to him for an advice. After that, I can get some idea to continue my work and the research program do work at last.

Finally, I would like to give a great big thank to Asst. Prof. Marija Vucelja as my thesis committee. She is also my teacher from the Mathematics method I class. I was impressed by her teaching style and opening class discussion. I appreciated for her time, understanding, spending her energy to read my thesis and advising suggestions as well.

Contents

List of Figures

List of Tables

Chapter 1

Introduction

High energy physics studies at present colliders involve both increasingly higher energies of the colliding beams and high luminosity which, in turn, can be accomplished using innovative and expensive equipment. Even though the Large Hadron Collider(LHC) can be used to study very high energy collisions, up to 13.6 TeV, and the Electron Ion Collider (EIC) will probe nucleons and nuclei at the highest luminosity, there is no limit to the inquisitiveness of humanity. What physics can be discovered at even higher energies and what unknowns aspects of all interacting subatomic matter would we like to to explore?

The evolution equations in perturbative Quantum Chromodynamics (pQCD) are one of the many ingredients that help determining the worthiness to build experimental colliders in a, so far, unexplored range of energy. Many physicists can use the evolution equations to explore these new regions, which will be soon at reach with current technology, unraveling both interesting behavior from pQCD evolution and perhaps new physics.

The pQCD evolution equations in this thesis are mainly used with parton distribution functions (PDFs) and subsequently applied to generalized parton distribution (GPD). The PDFs are an important ingredient for high energy predictions. The PDFs are extracted from experimental data at a given four-momentum scale, Q^2, by devising a parameterization with fitted parameters. The evolution process requires PDFs

calculated at an initial four-momentum scale, Q_o^2. Solving the equations allows us to connect the PDFs at the initial scale, Q_o^2, with the scale of the measurement that is interesting for experimental comparison, Q^2.

This thesis focuses on improving the efficiency – measured in both accuracy and calculation speed – of the numerical programming of the pQCD evolution equations. We focused on the Adams method to improve the efficiency. Python was chosen to be the main programming language. Indeed, there exist many previous numerical programs which cannot be used efficiently in global analyses because they are based on FORTRAN-77. Due to its user friendly nature Python is widely considered the univeral computer language.

Moreover, with the aim of helping new students in high energy and nuclear physics, I provide many details clarifying the working of the fundamental equations underlying pQCD evolution, which are quite intricate and not shown in mainstream textbooks.

The outline of the thesis consists of the following points:
- a brief introduction to the evolution equations in pQCD and necessary background knowledge.
- introduction to the Adams method for solving differential equations and the new form of generalized Adams method which I found during my thesis work.
- A step-by-step checklist as a useful tool for whoever is interested in reproducing results in pQCD evolution.
- Results from a comparison of the efficiencies of the Adams method with the Runge-Kutta 4(RK4), the most popular method and the Backward difference, the first order difference of the Adams method.
- Extension of results to GPD evolution and comparison to sum rules.
- Discussion of results.

- Summary of the interesting features found in my numerical study.

Chapter 2

QCD Physics and Evolution

2.1 History of Nuclear Physics through QCD

After humanity learned about atomic structure, a variety of fields were discovered. One of these is nuclear physics or the study of atomic nuclei and their substructures and interactions. These interactions happen at five orders of magnitude smaller distance scales compared to the scales of atomic physics.

The first essential discovery came from Henri Becquerel who discovered radioactivity of uranium salts in 1896. This discovery subsequently inspired other physicists including J.J. Thompson and Ernest Rutherford to perform more in depth studies of radioactivity and particle scattering. In 1911 Rutherford interpreted a most famous experiment in nuclear physics on the scattering of alpha particles off a gold foil performed by Hans Geiger and Ernest Marsden, who were his students. Based on the angular distribution of the scattered alpha particles, Rutherford discovered that the positively charged particles inside the atom where concentrated in a small volume defining the atomic nucleus. A long list of discoveries followed afterwards among which we mention Eddington's stellar nuclear fusion, Rasetti's nuclear spin, Chacwick's discovery of the neutron, Proca's equations of the massive vector boson field and Yukawa's meson.

In the years that followed, nuclear experiments were performed at higher and higher energies, requiring the use of special relativity for the description of the scattering processes as well as for the interpretation of all experiments. Antiparticles were discovered, thus allowing for novel particles production in the laboratory. But the question remained of what was the origin the newly discovered particles which were all subject to the strong interaction.

2.1.1 The Prediction and Discovery of Quarks and Gluons

In 1961, Murray Gell-Mann introduced a symmetry of the strong interaction in particle physics called the Eightfold Way or SU(3). The SU(3) symmetry required three new elementary particles.

In 1964, Gell-Mann and George Zweig, independently proposed that the three elementary particles would be identified as "quarks". In 1968, the MIT-SLAC collaboration revealed the first signs of the existence of the inner structure of a nucleon by the electron-proton scattering experiments. This discovery then was combined with the results from neutrino-scattering in the Gargamelle bubble chamber at CERN. The combination clearly showed that these particle had fractional charges of 2/3 (u quarks) and -1/3 (d quarks), as a predicted from the SU(3) model of quarks.

The prediction of gluons as carrier of the strong interactions was confirmed by the experiments only much later, in 1979 in electron-positron collision experiment at the collider PETRA of DESY, Germany.

The discovery of the gluon, or the mediator between the strong interactions among quarks, marks the origin of Quantum ChromoDynamics(QCD), the theory of strong interactions, which is modeled in analogy to Quantum ElectroDynamics(QED). Quarks and gluons, as consituents of all strongly interactiong particles (the hadrons) were

defined as “partons” by Richard Feynmann.

The number and momentum distribution of gluons in the proton were measured by H1 and ZEUS. The gluon contribution and gluon density to the proton spin was studied by the HERMES experiment at HERA.

Color confinement is verified by the failure of free quark searches. Even if quarks are produced in pairs (quark-antiquark) these hadronize, or they transform into mesons. Deconfinement is also possible, as investigated in heavy-ion collisions at CERN, but only in a new state of matter called Quark-Gluon Plasma (QGP) which is defined as an extremely hot “soup” of quarks and gluons.

The US Department of Energy facilities funds several facilities to research strongly interacting systems and the role of gluons. One of them is, in particular, Jefferson Laboratory’s Continuous Electron Beam Accelerator Facility in Virginia.

2.2 Bjorken Scaling Variable

The Bjorken scaling variable (X_{Bj}), introduced by James Bjorken in 1969, is the most essential kinematic building block for the parton distribution functions (PDFs) and QCD evolution equation.

Let us introduce X_{Bj} by both the kinematics and Feynman diagram underlying a deep inelastic scattering event.

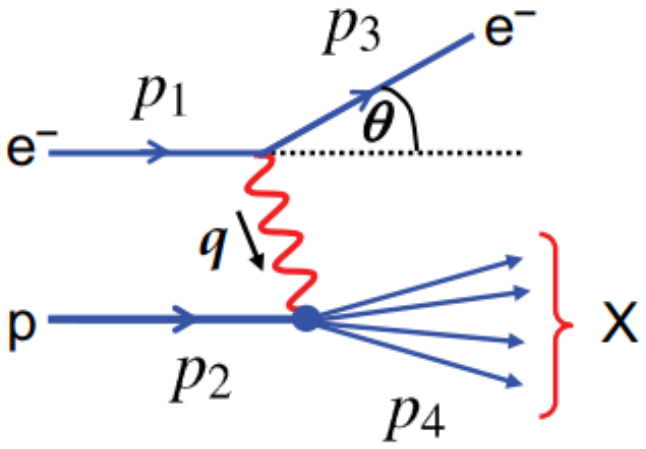

Figure 2.1: Kinematics

Bjorken x was defined as

$$X_{Bj} = x = \frac{Q^2}{2p_2 \cdot q} \tag{2.1}$$

X_{Bj} is the momentum fraction that the parton takes of the incoming proton longitudinal momentum. At the same time, it provides a measure of the elasticity or inelasticity of the scattering process.

Defining the final state invariant mass $W > M$, as,

$$W^2 = {p_4}^2 = ({E_4}^2 - |\vec{p_4}|^2) \tag{2.2}$$

where $Q^2 \equiv -q^2$ and $Q^2 > 0$

$$\begin{aligned} W^2 = {p_4}^2 = (q + p_2)^2 = -Q^2 + 2p_2 \cdot q + M^2 \\ Q^2 = 2p_2 \cdot q + M^2 - W^2 \end{aligned} \tag{2.3}$$

Including the proton intact case, $W = M$

$$Q^2 \leq 2p_2 \cdot q \tag{2.4}$$

refer to eq.(2.1),

$$\begin{aligned} 0 < x < 1 &\rightarrow inelastic \\ x = 1 &\rightarrow elastic \end{aligned} \tag{2.5}$$

Finally, define the energy lost by the incoming particle as

$$\nu \equiv \frac{p_2 q}{M} \tag{2.6}$$

Therefore, X_{Bj} takes the following form:

$$x = \frac{Q^2}{2M\nu} \tag{2.7}$$

2.3 Parton Distribution Functions and Parameterized Equation

The Parton Distribution Functions is the momentum distribution of partons (quarks and gluons) inside a proton.

PDFs cannot be calculated from first principles, namely, knowing the QCD Lagrangian, but they have to be determined from experiment. In practice one uses a fitting method, or parameterization, on a large set of cross section data points. Various criteria, or benchmarking, underlying the parametrizations definitions, including, for instance the initial conditions for PQCD evolution, have been set up at

the Les Houches meeting (reference).

In this thesis we use as a typical parametrization, the one from CTEQ5M parametrization given at the initial four-momentum scale,

$$Q_0^2 = 2 \text{ GeV}^2 \tag{2.8}$$

The distributions are,

$$\begin{aligned}
xu_v(x,{Q_0}^2) &= 5.107200x^{0.8}(1-x)^3 && (2.9)\\
xd_v(x,{Q_0}^2) &= 3.064320x^{0.8}(1-x)^4 && (2.10)\\
xg(x,{Q_0}^2) &= 1.700000x^{-0.1}(1-x)^5 && (2.11)\\
x\overline{d}(x,{Q_0}^2) &= 0.1939875x^{-0.1}(1-x)^6 && (2.12)\\
x\overline{u}(x,{Q_0}^2) &= (1-x)xd_v(x,{Q_0}^2) && (2.13)\\
xs(x,{Q_0}^2) &= x\overline{s}(x,{Q_0}^2) = 0.2x(\overline{u}+\overline{d})(x,{Q_0}^2) && (2.14)
\end{aligned}$$

Let us look at the above initial distributions. For instance, the pattern of PDFs might be assumed to be

$$xPDF(x,{Q_0}^2) = ax^b(1-x)^c, \tag{2.15}$$

however, the pattern of parameterization might be in other forms. Here one introduces a model dependence on the initial parameterization which is, however, mitigated by the fact that all of the parameterized xPDFs are subject to various constraints, including, for example the baryon number and momentum conservation sum rules.

2.4 Mellin Moment

The moment of non-singlet structure functions have a Q^2 dependence given by

$$M_n{}^{NS}(Q^2) = \int_0^1 dx x^{n-2} F_2^{NS}(x, Q^2) = M_n{}^{NS}({Q_0}^2) \left[\frac{\alpha_s(Q^2)}{\alpha_s({Q_0}^2)} \right]^{d_n^{NS}} \tag{2.16}$$

where the $d_n^{NS} = \gamma_0^{n,NS}/2\beta_0$ Note that at n=1, Mellin moment is a total number of quarks and gluon inside the structure function.

In addition, the α_s of the running constant is in this form.

$$\alpha_s(Q^2) = \frac{4\pi}{\beta_0 \ln(Q^2/\Lambda^2)} \tag{2.17}$$

and

$$\beta_0 = 11 - \frac{2}{3} N_f \tag{2.18}$$

We should notice that the running constant changes with Q^2. The energy level $Q^2 \leq {m_c}^2$, $N_f = 3$. Then, when ${m_c}^2 \leq Q^2 \leq {m_b}^2$, $N_f = 4$. Lastly, when ${m_b}^2 \leq Q^2$, $N_f = 5$.

Moreover, there are more corresponding corrections of $\Lambda_{(N_f)}$ which can be described with the set of following equations and a number of flavors.

$$\begin{aligned} \Lambda_{(3)} &= \Lambda_{(4)} \left(\frac{m_c}{\Lambda_{(4)}} \right)^{\frac{2}{27}} \\ \Lambda_{(5)} &= \Lambda_{(4)} \left(\frac{m_b}{\Lambda_{(4)}} \right)^{-\frac{2}{23}} \end{aligned} \tag{2.19}$$

Where $\Lambda_{(4)} \approx 200$ MeV for a proton, $m_{(c)} = 2\ GeV^2$, $m_{(b)} = 4.5\ GeV^2$,
and $m_{(t)} = 175\ GeV^2$

2.5 DGLAP Equation

The Dokshitzer–Gribov–Lipatov–Altarelli–Parisi (DGLAP) evolution equations describe the variation of parton distribution function at different energy/four-momentum squared.

Look at the Deep Inelastic Scattering (DIS) diagram below. Let us focus on the upper right vertex of each diagram. There are four splitting types.

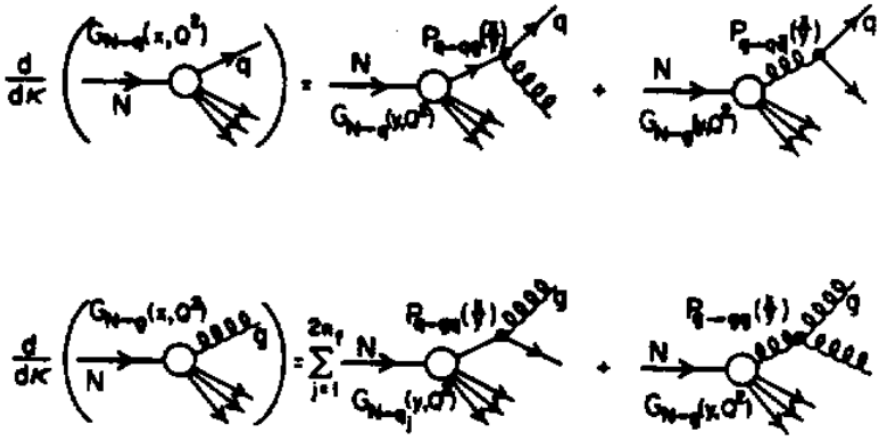

Figure 2.2: Splitting functions illustration [Field and Pines 1995]

The splitting function determines the probability of quark-gluon radiation. As you can see from the diagrams, the upper 2 splitting types are P_{qq} and P_{qG} which the first q is the outcoming quark and the second one indicates the incoming quark and gluon respectively.

Similarly, the lower two splitting types are are P_{Gq} and P_{GG} which the first G is the out-coming gluon and another is the incoming parton.

For example, the P_{qq} evolution only case can be written in this following form. This case is also called Non-Singlet(NS) structure function case, where the Non-singlet

structure function is a measured structure function of partons with the valence quark number.

$$\frac{d}{d\ln Q^2} f_q(x,Q^2) = C_F \frac{\alpha_S}{2\pi} \int_x^1 dy\, f_q(y,Q^2)\, P_{qq} \tag{2.20}$$

And the full formula is,

$$\begin{aligned} \frac{d}{d\ln Q^2} f_q(x,Q^2) &= C_F \frac{\alpha_S}{2\pi} \Bigg[\int_x^1 \frac{dy}{y} \frac{\left[1+\left(\frac{x}{y}\right)^2\right] f_q(y,Q^2) - 2 f_q(x,Q^2)}{1-\frac{x}{y}} \\ &+ f_q(x,Q^2) \left(2\ln(1-x) + \frac{3}{2}\right) \Bigg] \end{aligned} \tag{2.21}$$

where we introduced the notation, f_q, for the parton distribution, labeling the different quark types with: $q = u, d, s, c, b$.

The reason why the formula is lengthy is because the PDFs are written in terms of the auxilliary variables, $x - y$ dependence, replacing the z dependence.

Next, let us derive the DGLAP equation with P_{qq}, P_{gg}, P_{qg} and P_{gq} in term of x and y.

2.5.1 Derivation of DGLAP Equation with P_{qq}

The P_{qq} in term of z can be written as,

$$P_{qq} = C_F \left[\frac{1+z^2}{(1-z)_+} + \frac{3}{2}\delta(1-z) \right] \tag{2.22}$$

and the DGLAP equation with P_{qq} function is,

$$\frac{dq^{NS}(x,Q^2)}{d\ln Q^2} = \frac{\alpha_s}{2\pi}\int_x^1 \frac{dy}{y} P_{qq}(z) q^{NS}(y,Q^2) \tag{2.23}$$

$$\frac{dq^{NS}(x,Q^2)}{d\ln Q^2} = \frac{\alpha_s}{2\pi}\int_x^1 \frac{dy}{y} C_F \left[\frac{1+z^2}{(1-z)_+} + \frac{3}{2}\delta(1-z) \right] q^{NS}(y,Q^2) \tag{2.24}$$

$$\frac{1}{x}\frac{dxq^{NS}(x,Q^2)}{d\ln Q^2} = \frac{\alpha_s}{2\pi}\int_x^1 \frac{dy}{y^2} C_F \left[\frac{1+z^2}{(1-z)_+} + \frac{3}{2}\delta(1-z) \right] yq^{NS}(y,Q^2) \tag{2.25}$$

By the definition of a structure function,

$$F^{NS}(y,Q^2) = yq(y,Q^2), F^{NS}(x,Q^2) = xq(x,Q^2) \tag{2.26}$$

Then, eq.(2.25) becomes,

$$\frac{1}{x}\frac{dF^{NS}(x,Q^2)}{d\ln Q^2} = \frac{\alpha_s}{2\pi}\int_x^1 \frac{dy}{y^2} C_F \left[\frac{1+z^2}{(1-z)_+} + \frac{3}{2}\delta(1-z) \right] F^{NS}(y,Q^2) \tag{2.27}$$

$$\frac{dF^{NS}(x,Q^2)}{d\ln Q^2} = \frac{\alpha_s}{2\pi}\int_x^1 \frac{xdy}{y^2} C_F \left[\frac{1+z^2}{(1-z)_+} + \frac{3}{2}\delta(1-z) \right] F^{NS}(y,Q^2) \tag{2.28}$$

the relation of x, y and z can be written as $z = \dfrac{x}{y}$

$$\frac{dz}{dy} = \frac{y\dfrac{dx}{dy} - x\dfrac{dy}{dy}}{y^2} = -\frac{x}{y^2} \tag{2.29}$$

Thus,

$$dz = -\frac{x}{y^2}dy \tag{2.30}$$

and $z = \dfrac{x}{y}$ defines the limit of the integral at $y = 1$, $z = x$ and when $y = x$, $z = 1$.

Then, Eq.(2.28) becomes,

$$\frac{dF^{NS}(x,Q^2)}{dlnQ^2} = -C_F\frac{\alpha_s}{2\pi}\int_1^x dz\left[\frac{1+z^2}{(1-z)_+} + \frac{3}{2}\delta(1-z)\right]F^{NS}\left(\frac{x}{z},Q^2\right) \tag{2.31}$$

Afterward, let us switch the integral limit from $z = 1$ to $z = x$ into $z = x$ to $z = 1$, using this relation,

$$\int_a^b f(x)dx = -\int_b^a f(x)dx \tag{2.32}$$

$$\frac{dF^{NS}(x,Q^2)}{d\ln Q^2} = C_F\frac{\alpha_s}{2\pi}\int_x^1 dz\left[\frac{1+z^2}{(1-z)_+} + \frac{3}{2}\delta(1-z)\right]F^{NS}\left(\frac{x}{z},Q^2\right) \tag{2.33}$$

$$\frac{dF^{NS}(x,Q^2)}{d\ln Q^2} = C_F\frac{\alpha_s}{2\pi}\int_x^1 dz\left[\frac{1+z^2}{(1-z)_+}F^{NS}\left(\frac{x}{z},Q^2\right) + \frac{3}{2}\delta(1-z)F^{NS}\left(\frac{x}{z},Q^2\right)\right] \tag{2.34}$$

In the next step, let consider the plus function,

$$\int_x^1 dz\frac{f(\frac{x}{z})}{(1-z)_+} = \int_0^1 dz\frac{f(\frac{x}{z})}{(1-z)_+} - \int_0^x dz\frac{f(\frac{x}{z})}{(1-z)_+} \tag{2.35}$$

and the definition of the plus function is,

$$\int_0^1 dz \frac{f(z)}{(1-z)_+} = \int_0^1 dz \frac{f(z)-f(1)}{1-z} \tag{2.36}$$

Then, Eq.(2.35) becomes,

$$\int_x^1 dz \frac{f(\frac{x}{z})}{(1-z)_+} = \int_0^1 dz \frac{f(\frac{x}{z})-f(\frac{x}{1})}{1-z} - \int_0^x dz \frac{f(\frac{x}{z})-f(\frac{x}{x})}{1-z} \tag{2.37}$$

$$\int_x^1 dz \frac{f(\frac{x}{z})}{(1-z)_+} = \int_0^1 dz \frac{f(\frac{x}{z})-f(x)}{1-z} - \int_0^x dz \frac{f(\frac{x}{z})-f(1)}{1-z}. \tag{2.38}$$

As the definition of the plus function (see Appendix), the function which is convoluted with the plus function will reach 0 as x approachws 1. Therefore, $f(1) = 0$. Next, Eq.(2.38) is,

$$\int_x^1 dz \frac{f(\frac{x}{z})}{(1-z)_+} = (\int_x^1 dz \frac{f(\frac{x}{z})-f(x)}{1-z} + \int_0^x dz \frac{f(\frac{x}{z})-f(x)}{1-z}) - \int_0^x dz \frac{f(\frac{x}{z})}{1-z} \tag{2.39}$$

$$\int_x^1 dz \frac{f(\frac{x}{z})}{(1-z)_+} = \int_x^1 dz \frac{f(\frac{x}{z})-f(x)}{1-z} - \int_0^x dz \frac{f(x)}{1-z} \tag{2.40}$$

$$\int_x^1 dz \frac{f(\frac{x}{z})}{(1-z)_+} = \int_x^1 dz \frac{f(\frac{x}{z})-f(x)}{1-z} + ln(1-x)f(x) \tag{2.41}$$

with the help of Eq.(2.41) where,

$$f\left(\frac{x}{z}\right) = F^{NS}\left(\frac{x}{z}, Q^2\right)(1+z^2) \tag{2.42}$$

Consider 1^{st} term of Eq.(2.34),

$$C_F \frac{\alpha_s}{2\pi} \int_x^1 dz F^{NS}\left(\frac{x}{z}, Q^2\right) \frac{1+z^2}{(1-z)_+}$$

$$= C_F \frac{\alpha_s}{2\pi} \Bigg\{ \int_x^1 dz \frac{F^{NS}\big(\frac{x}{z}, Q^2\big)(1+z^2) - F^{NS}\big(x, Q^2\big)(1+1^2)}{1-z} + ln(1-x) F^{NS}\big(x, Q^2\big)(1+1^2) \Bigg\}$$

$$= C_F \frac{\alpha_s}{2\pi} \Bigg\{ \int_x^1 \frac{dz}{1-z} \Big[(1+z^2) F^{NS}\big(\frac{x}{z}, Q^2\big) - 2F^{NS}\big(x, Q^2\big) \Big] + 2ln(1-x) F^{NS}\big(x, Q^2\big) \Bigg\} \tag{2.43}$$

and the 2^{nd} term,

$$C_F \frac{\alpha_s}{2\pi} \int_x^1 dz \frac{3}{2} \delta(1-z) F^{NS}\left(\frac{x}{z}, Q^2\right) = C_F \frac{\alpha_s}{2\pi} \left(\frac{3}{2} F^{NS}\big(x, Q^2\big) \right) \tag{2.44}$$

Finally,

$$\begin{aligned} \frac{dF^{NS}(x,Q^2)}{d\ln Q^2} &= C_F \frac{\alpha_s}{2\pi} \Bigg\{ \int_x^1 \frac{dz}{1-z} \Big[(1+z^2) F^{NS}\big(\frac{x}{z}, Q^2\big) - 2F^{NS}\big(x, Q^2\big) \Big] \\ &+ \left[\frac{3}{2} + 2\ln(1-x) \right] F^{NS}\big(x, Q^2\big) \Bigg\} \end{aligned} \tag{2.45}$$

2.5.2 Derivation of DGLAP Equation with P_{GG}

The P_{GG} in term of z can be written as,

$$P_{GG} = 2C_A \left[\frac{z}{(1-z)_+} + \frac{1-z}{z} + z(1-z) \right] + \frac{1}{2} \beta_0 \delta(1-z) \tag{2.46}$$

and the DGLAP equation with P_{GG} function is

$$\frac{dg(x,Q^2)}{d\ln Q^2} = \frac{\alpha_s}{2\pi} \int_x^1 \frac{dy}{y} P_{GG}(z) g(y, Q^2) \tag{2.47}$$

$$\frac{1}{x} \frac{dxg(x,Q^2)}{dlnQ^2} = \frac{\alpha_s}{2\pi} \int_x^1 \frac{dy}{y^2} P_{GG}(z) y g(y, Q^2) \tag{2.48}$$

$$\frac{1}{x}\frac{dG(x,Q^2)}{d\ln Q^2} = \frac{\alpha_s}{2\pi}\int_x^1 \frac{dy}{y^2}G(y,Q^2)\Big\{2C_A\Big[\frac{z}{(1-z)_+}+\frac{1-z}{z}+z(1-z)\Big]+\frac{1}{2}\beta_0\delta(1-z)\Big\} \tag{2.49}$$

$$\frac{dG(x,Q^2)}{d\ln Q^2} = \frac{\alpha_s}{2\pi}\int_x^1 \frac{xdy}{y^2}G(y,Q^2)\Big\{2C_A\Big[\frac{z}{(1-z)_+}+\frac{1-z}{z}+z(1-z)\Big]+\frac{1}{2}\beta_0\delta(1-z)\Big\} \tag{2.50}$$

as the same step as in P_{qq} case,

$$\frac{dG(x,Q^2)}{d\ln Q^2} = \frac{\alpha_s}{2\pi}\int_x^1 dzG\Big(\frac{x}{z},Q^2\Big)\Big\{2C_A\Big[\frac{z}{(1-z)_+}+\frac{1-z}{z}+z(1-z)\Big]+\frac{1}{2}\beta_0\delta(1-z)\Big\} \tag{2.51}$$

Let focus on the 1^{st} term,

$$\frac{\alpha_s}{2\pi}\int_x^1 dzG\Big(\frac{x}{z},Q^2\Big)2C_A\Big[\frac{z}{(1-z)_+}\Big] = \frac{C_A\alpha_s}{\pi}\int_x^1 dz\frac{zG\big(\frac{x}{z},Q^2\big)}{(1-z)_+} \tag{2.52}$$

with the help of Eq.(2.41) where,

$$f(\frac{x}{z}) = zG\Big(\frac{x}{z},Q^2\Big) \tag{2.53}$$

After evaluating it, Eq.(2.52) will be,

$$\frac{C_A\alpha_s}{\pi}\int_x^1 dz\frac{zG\big(\frac{x}{z},Q^2\big)}{(1-z)_+} = \frac{C_A\alpha_s}{\pi}\Big[\int_x^1 dz\frac{zG\big(\frac{x}{z},Q^2\big)-G\big(x,Q^2\big)}{1-z}+\ln(1-x)G\big(x,Q^2\big)\Big]. \tag{2.54}$$

Then, all terms become,

$$\frac{dG(x,Q^2)}{d\ln Q^2} = \frac{\alpha_s}{2\pi}\int_x^1 dzG\Big(\frac{x}{z},Q^2\Big)\Big\{2C_A\Big[\frac{z}{(1-z)_+}+\frac{1-z}{z}+z(1-z)\Big]+\frac{1}{2}\beta_0\delta(1-z)\Big\} \tag{2.55}$$

$$\frac{dG(x,Q^2)}{d\ln Q^2} = \frac{C_A\alpha_s}{\pi}\Big\{\int_x^1 dz\Big[\frac{zG\Big(\frac{x}{z},Q^2\Big)}{(1-z)_+}+\int_x^1 dz\Big[\frac{1-z}{z}+z(1-z)\Big]G\Big(\frac{x}{z},Q^2\Big)\Big\}+\frac{\alpha_s}{4\pi}\beta_0 G\big(x,Q^2\big) \tag{2.56}$$

$$\begin{aligned}\frac{dG(x,Q^2)}{d\ln Q^2} = \frac{C_A\alpha_s}{\pi}\Bigg\{\Big[\int_x^1 dz\frac{zG\big(\frac{x}{z},Q^2\big)-G\big(x,Q^2\big)}{1-z}+ln(1-x)G\big(x,Q^2\big)\Big] \\ +\int_x^1 dz\Big[\frac{1-z}{z}+z(1-z)\Big]G\Big(\frac{x}{z},Q^2\Big)\Bigg\}+\frac{\alpha_s}{4\pi}\beta_0 G\big(x,Q^2\big)\end{aligned} \tag{2.57}$$

Therefore, the DGLAP equation for P_{GG} case is,

$$\begin{aligned}\frac{dG(x,Q^2)}{d\ln Q^2} = \frac{C_A\alpha_s}{\pi}\Bigg\{\int_x^1 dz\Big[\frac{z}{1-z}+\frac{1-z}{z}+z(1-z)\Big]G\Big(\frac{x}{z},Q^2\Big)-\frac{G\big(x,Q^2\big)}{1-z}\Bigg\} \\ +\frac{\alpha_s}{4\pi}\beta_0 G\big(x,Q^2\big)+\frac{C_A\alpha_s}{\pi}\ln(1-x)G\big(x,Q^2\big)\end{aligned} \tag{2.58}$$

2.5.3 Derivation of DGLAP Equation with P_{qG}

The P_{qG} in term of z can be written as,

$$P_{qG} = T_F[z^2+(1-z)^2] \tag{2.59}$$

and the DGLAP equation with P_{qG} function is

$$\frac{dg(x,Q^2)}{d\ln Q^2} = \frac{\alpha_s}{2\pi}\int_x^1\frac{dy}{y}P_{qG}(z)g(y,Q^2) \tag{2.60}$$

$$\frac{dg(x,Q^2)}{d\ln Q^2} = \frac{\alpha_s}{2\pi}\int_x^1\frac{dy}{y}T_F[z^2+(1-z)^2]g(y,Q^2) \tag{2.61}$$

$$\frac{1}{x}\frac{dxg(x,Q^2)}{dlnQ^2} = T_F\frac{\alpha_s}{2\pi}\int_x^1 \frac{dy}{y^2}[z^2+(1-z)^2]yg(y,Q^2) \tag{2.62}$$

$$\frac{dG(x,Q^2)}{d\ln Q^2} = T_F\frac{\alpha_s}{2\pi}\int_x^1 \frac{xdy}{y^2}[z^2+(1-z)^2]G(y,Q^2) \tag{2.63}$$

Finally, changing a variable y into x,z

$$\frac{dG(x,Q^2)}{d\ln Q^2} = T_F\frac{\alpha_s}{2\pi}\int_x^1 dz[z^2+(1-z)^2]G\left(\frac{x}{z},Q^2\right) \tag{2.64}$$

2.5.4 Derivation of DGLAP Equation with P_{Gq}

The P_{Gq} in term of z can be written as,

$$P_{Gq} = C_F\left[\frac{1+(1-z)^2}{z}\right] \tag{2.65}$$

and the DGLAP equation with P_{Gq} function is

$$\frac{dq(x,Q^2)}{dlnQ^2} = \frac{\alpha_s}{2\pi}\int_x^1 \frac{dy}{y}P_{Gq}(z)q(y,Q^2) \tag{2.66}$$

$$\frac{1}{x}\frac{dxq(x,Q^2)}{d\ln Q^2} = \frac{\alpha_s}{2\pi}\int_x^1 \frac{dy}{y^2}P_{Gq}(z)yq(y,Q^2) \tag{2.67}$$

$$\frac{dF(x,Q^2)}{d\ln Q^2} = \frac{\alpha_s}{2\pi}\int_x^1 \frac{xdy}{y^2}P_{Gq}(z)F(y,Q^2) \tag{2.68}$$

The final equation for a P_{Gq} case is

$$\frac{dF(x,Q^2)}{d\ln Q^2} = C_F\frac{\alpha_s}{2\pi}\int_x^1 dz\left[\frac{1+(1-z)^2}{z}\right]F\left(\frac{x}{z},Q^2\right) \tag{2.69}$$

2.6 Sum Rules

The splitting functions have their conservation rules. The thesis use the following four rules to indicate the correction of the program.

These rules are

$$\begin{gathered}\int_0^1 dz P_{qq}(z) = 0 \\ \int_0^1 dz u_v(z,Q^2), = 2 \qquad \int_0^1 dz d_v(z,Q^2) = 1 \\ \int_0^1 dz z[P_{qq}(z) + P_{Gq}(z)] = 0 \\ \int_0^1 dz z[2N_f P_{qG}(z) + P_{GG}(z)] = 0\end{gathered} \tag{2.70}$$

where we define the valence/flavor non-singlet NS, quarks as $u_v = u(x,Q^2) - \bar{u}(x,Q^2)$, and $d_v = d(x,Q^2) - \bar{d}(x,Q^2)$.

The first rule just come from the integration of $P_{qq}(z)$ which I will show herebelow,

$$\int_0^1 dz P_{qq}(z) = \int_0^1 dz \left[\frac{1+z^2}{(1-z)_+} + \frac{3}{2}\delta(1-z) \right] \tag{2.71}$$

with the definition of the plus function, the eq.(2.71) becomes,

$$\begin{aligned}
\int_0^1 dz P_{qq}(z) &= \int_0^1 dz \frac{1+z^2-(1+1^2)}{1-z} + \frac{3}{2} \\
&= \int_0^1 dz \frac{1+z^2-2}{1-z} + \frac{3}{2} \\
&= \int_0^1 dz - \frac{1-z^2}{1-z} + \frac{3}{2} \\
&= \int_0^1 dz - (1+z) + \frac{3}{2} \\
&= -\left[z + \frac{z^2}{2}\right]_{z=0}^{z=1} + \frac{3}{2} = 0
\end{aligned} \tag{2.72}$$

2.7 Generalized Parton Distribution Function

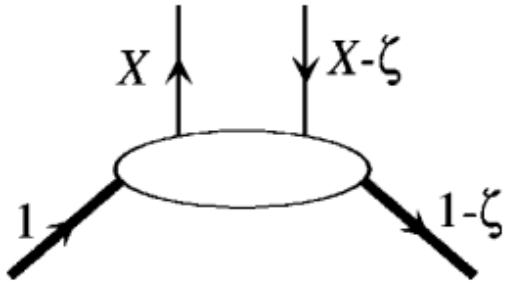

Figure 2.3: The proton and quark momentum fractions with respect to the initial proton momentum P corresponding to the off-diagonal distributions $\hat{F}(X,z)$ defined in the domain 0<X<1. [Golec-Biernat and Martin 1999]

The asymmetry of the scattering show the new variable describing the new parton distribution function. The new functions are know as Generalized Parton Density(GPD). An extension to the higher dimension allow us to explore the more generalized cases in the nature. Indeed, The GPD($\hat{F}(x,\zeta,Q^2)$) is different from PDF($F(x,Q^2)$). The GPD using in the thesis is the special case of $\zeta = 0$. Then, $\hat{F}(x,\zeta,Q^2) = F(x,Q^2)$)

Therefore ,the evolution equation of the Non-singlet case becomes

$$\frac{\partial F^{NS}(x,\zeta,Q^2)}{\partial lnQ^2} = C_F\frac{\alpha_s}{2\pi}\Bigg\{\int_x^1 \frac{dz}{1-z}\Big[(1+zz')F^{NS}\big(\frac{x}{z},Q^2\big) - (1+\frac{z'}{z})F^{NS}\big(x,Q^2\big)\Big] + \Big[\frac{3}{2} + ln\frac{(1-x)^2}{1-\zeta}\Big]F^{NS}\big(x,Q^2\big)\Bigg\} \tag{2.73}$$

Chapter 3

Adams' Method

3.1 Adams 2d and Linear x-space

The Adams' Method is the numerical method to solve a first order ordinary differential equation with this form,

$$\frac{dy}{dx} = f(x, y) \tag{3.1}$$

within range of $[a, b]$ and N steps of iteration with an assumption about every function can be expressed by an expansion of Taylor's series about the x_n,

$$y_{n+1} = y_(n) + (\frac{dy}{dx})_n (x - x_n) + \frac{1}{2}(\frac{d^2y}{dx^2})_n (x - x_n)^2 + ... \tag{3.2}$$

The derivatives of y are given by the backward difference

$$q_n \equiv (\frac{dy}{dx})_n = \frac{y_{n+1} - y_n}{x_{n+1} - x_n} \tag{3.3}$$

$$\nabla q_n \equiv (\frac{d^2y}{dx^2})_n = q_n - q_{n-1} \tag{3.4}$$

$$\nabla^2 q_n \equiv (\frac{d^3y}{dx^3})_n = \nabla q_n - \nabla q_{n-1} \tag{3.5}$$

For the higher orders, they can be obtained by using the same iterations.

To receive the same form as the Taylor's series, the Beyer's finite difference integration

formula can be used to extended to arbitrary order.

$$\int_0^1 f_p dp = (1 + \frac{1}{2}\nabla + \frac{5}{12}\nabla^2 + \frac{3}{8}\nabla^3 + \frac{251}{720}\nabla^4 + \frac{95}{288}\nabla^5 + \frac{19087}{60480}\nabla^6 + ...)f_p \quad (3.6)$$

Then,

$$y_{n+1} = y_n + H(q_n + \frac{1}{2}\nabla q_{n-1} + \frac{5}{12}\nabla^2 q_{n-2} + \frac{3}{8}\nabla^3 q_{n-3} + \frac{251}{720}\nabla^4 q_{n-4} + \frac{95}{288}\nabla^5 q_{n-5} + \frac{19087}{60480}\nabla^6 q_{n-6} + ...) \quad (3.7)$$

where $h = x_{n+1} - x_n = x_{n+2} - x_{n+1} = ...$

and $H = \frac{(b-a)}{N}$

Let expand q_n, ∇q_n , $\nabla^2 q_n$, $\nabla^3 q_n$,

$$q_n = (\frac{dy}{dx})_n = f(x_n, y_n) = \frac{1}{h}(y_{n+1} - y_n) \quad (3.8)$$

$$\nabla q_n = (\frac{d^2y}{dx^2})_n = q_n - q_{n-1} = \frac{y_{n+1} - y_n}{h} - \frac{y_n - y_{n-1}}{h}$$

$$\nabla q_n = \frac{1}{h}(y_{n+1} - 2y_n + y_{n-1}) \quad (3.9)$$

$$\nabla^2 q_n = (\frac{d^3y}{dx^3})_n = \nabla q_n - \nabla q_{n-1} = \frac{1}{h}(y_{n+1} - 2y_n + y_{n-1}) - \frac{1}{h}(y_n - 2y_{n-1} + y_{n-2})$$

$$\nabla^2 q_n = \frac{1}{h}(y_{n+1} - 3y_n + 3y_{n-1} - y_{n-2}) \quad (3.10)$$

$$\nabla^3 q_n = (\frac{d^4y}{dx^4})_n = \nabla^2 q_n - \nabla^2 q_{n-1} = \frac{1}{h}(y_{n+1} - 3y_n + 3y_{n-1} - y_{n-2}) - \frac{1}{h}(y_n - 3y_{n-1} + 3y_{n-2} - y_{n-3})$$

$$\nabla^3 q_n = \frac{1}{h}(y_{n+1} - 4y_n + 6y_{n-1} - 4y_{n-2} + y_{n-3}) \quad (3.11)$$

Let shift the subscripts to be ∇q_{n-1} , $\nabla^2 q_{n-2}$, $\nabla^3 q_{n-3}$,

$$\nabla q_{n-1} = \frac{1}{h}(y_n - 2y_{n-1} + y_{n-2}) \tag{3.12}$$

$$\nabla^2 q_{n-2} = \frac{1}{h}(y_{n-1} - 3y_{n-2} + 3y_{n-3} - y_{n-4}) \tag{3.13}$$

$$\nabla^3 q_{n-3} = \frac{1}{h}(y_{n-2} - 4y_{n-3} + 6y_{n-4} - 4y_{n-5} + y_{n-6}) \tag{3.14}$$

Afterward, eq. (7) becomes

$$y_{n+1} = y_n + H[f(x_n, y_n) + \frac{1}{2h}(y_n - 2y_{n-1} + y_{n-2}) + \frac{5}{12h}(y_{n-1} - 3y_{n-2} + 3y_{n-3} - y_{n-4})$$

$$+ \frac{3}{8h}(y_{n-2} - 4y_{n-3} + 6y_{n-4} - 4y_{n-5} + y_{n-6}) \tag{3.15}$$

All elements in (15) can be found by using,

$$x_{n-1} = x_n - h, \quad y_{n-1} = y_n - q_n h \tag{3.16}$$

The eq.(15) will be used with other more functions and compared these results with RK4 in next section.

3.2 Adams 2d and Nonlinear x-space

For a nonlinear x-space, the different between each x point is unequal. Then, the $q_n, \nabla q_n, \nabla^2 q_n$ must be written in other forms.

$$q_n \equiv (\frac{dy}{dx})_n = \frac{y_{n+1} - y_n}{x_{n+1} - x_n} \tag{3.17}$$

$$\nabla q_n \equiv (\frac{d^2y}{dx^2})_n = q_n - q_{n-1} = \frac{y_{n+1} - y_n}{x_{n+1} - x_n} - \frac{y_n - y_{n-1}}{x_n - x_{n-1}} \tag{3.18}$$

$$\nabla^2 q_n \equiv (\frac{d^3y}{dx^3})_n = \nabla q_n - \nabla q_{n-1} = [\frac{y_{n+1} - y_n}{x_{n+1} - x_n} - \frac{y_n - y_{n-1}}{x_n - x_{n-1}}] - [\frac{y_n - y_{n-1}}{x_n - x_{n-1}} - \frac{y_{n-1} - y_{n-2}}{x_{n-1} - x_{n-2}}] \tag{3.19}$$

$$\nabla^3 q_{n-3} = \nabla^2 q_n - \nabla^2 q_{n-1} =$$

$$[[\frac{y_{n+1} - y_n}{x_{n+1} - x_n} - \frac{y_n - y_{n-1}}{x_n - x_{n-1}}] - [\frac{y_n - y_{n-1}}{x_n - x_{n-1}} - \frac{y_{n-1} - y_{n-2}}{x_{n-1} - x_{n-2}}]] -$$

$$[[\frac{y_n - y_{n-1}}{x_n - x_{n-1}} - \frac{y_{n-1} - y_{n-2}}{x_{n-1} - x_{n-2}}] - [\frac{y_{n-1} - y_{n-2}}{x_{n-1} - x_{n-2}} - \frac{y_{n-2} - y_{n-3}}{x_{n-2} - x_{n-3}}]] \tag{3.20}$$

These equations are incredibly complicated and too long because the inequality in x-space cannot be written in the universal form. However, I found that these equation can be simplified like this.

$$q_n \equiv (\frac{dy}{dx})_n = f(x,y)_n \tag{3.21}$$

$$\nabla q_n \equiv (\frac{d^2y}{dx^2})_n = q_n - q_{n-1} = f(x,y)_n - f(x,y)_{n-1} \tag{3.22}$$

$$\nabla^2 q_n \equiv (\frac{d^3y}{dx^3})_n = \nabla q_n - \nabla q_{n-1}$$

$$= [f(x,y)_n - f(x,y)_{n-1}] - [f(x,y)_{n-1} - f(x,y)_{n-2}]$$

$$= f(x,y)_n - 2f(x,y)_{n-1} + f(x,y)_{n-2} \tag{3.23}$$

$$\nabla^3 q_{n-3} = \nabla^2 q_n - \nabla^2 q_{n-1} =$$

$$= [f(x,y)_n - 2f(x,y)_{n-1} + f(x,y)_{n-2}] - [f(x,y)_{n-1} - 2f(x,y)_{n-2} + f(x,y)_{n-3}]$$

$$= f(x,y)_n - 3f(x,y)_{n-1} + 3f(x,y)_{n-2} - f(x,y)_{n-3} \tag{3.24}$$

Therefore, the whole Adams' equation can be written in the following form.

$$y_{n+1} = y_n + h[f(x_n,y_n) + \frac{1}{2}(f(x,y)_n - f(x,y)_{n-1}) + \frac{5}{12}(f(x,y)_n - 2f(x,y)_{n-1} + f(x,y)_{n-2})$$

$$+ \frac{3}{8}(f(x,y)_n - 3f(x,y)_{n-1} + 3f(x,y)_{n-2} - f(x,y)_{n-3}) \tag{3.25}$$

3.3 Toy Model Functions

The toy models we implemented are functions of $\sin(x)$, $\cos(x)$, $\exp(x)$, $exp(-x)$, as well as polynomials in x and Gaussian functions. The scope of the toy models study is to determine the capability of the Adams method to improve the numerical efficiency of the integro-differential evolution equations.

These functions are defined as $f(x)$ and tested with Adams' method, RK4 and Backward Difference (BD). The results are described below.

I firstly used the polynomials of order 3-6, obtaining the results displayed in Figures 3.1a, 3.1b, 3.1c, 3.1d, 3.1e, 3.1f, 3.1g and 3.1h, for the polynomial of order 3; in Figures 3.2a, 3.2b, 3.2c, 3.2d, 3.2e, 3.2f, 3.2g, 3.2h, for the polynomial of order 4; 3.3a, 3.3a, 3.3b, 3.3c, 3.3d, 3.3e, 3.3f, 3.3g, 3.3g, 3.3h, for the polynomials of order 5; for the polynomial of order 5, and finally, 3.4a, 3.4b, 3.4c, 3.4d, 3.4e, 3.4f, 3.4g, 3.4h, for the polynomials of order 5 for the polynomial or order 6.

In each figure the upper panels, labeled $a - d$, show the numerical evaluations com-

pared with the known, analytic value of the function, $g(x)$, increasing the number of steps from 10 to 100. The lower panels, labeled $e - h$, show the error for the corresponding number of steps. From these results we conclude that the Adams' and BD method are more precise than RK4, for all order polynomials. Note that the erros increase with x.

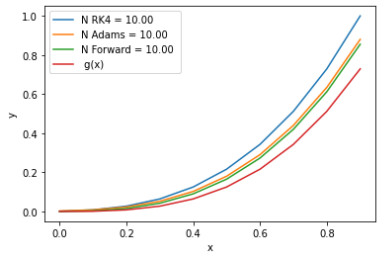

(a) numerical calculation of $g(x) = x^3$ with the number of step = 10

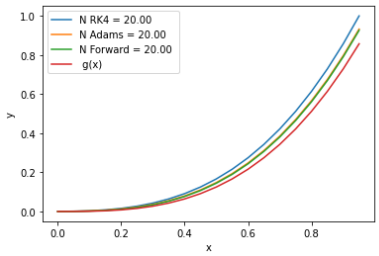

(b) numerical calculation of $g(x) = x^3$ with the number of step = 20

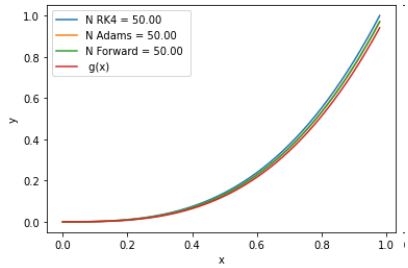

(c) numerical calculation of $g(x) = x^3$ with the number of step = 50

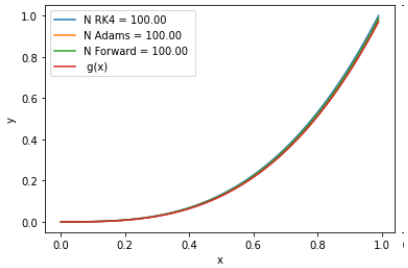

(d) numerical calculation of $g(x) = x^3$ with the number of step = 100

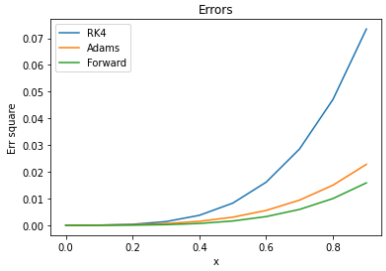

(e) Absolute error of $g(x) = x^3$ with the number of step = 10

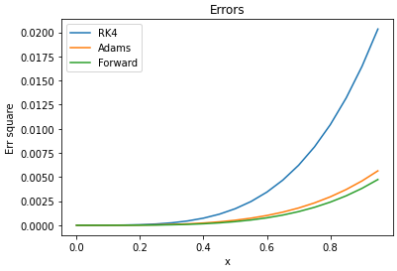

(f) Absolute error of $g(x) = x^3$ with the number of step = 20

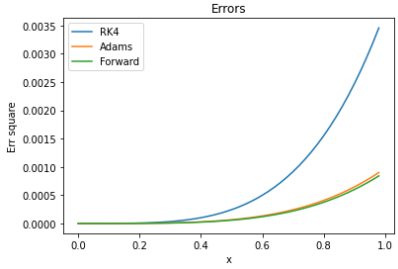

(g) Absolute error of $g(x) = x^3$ with the number of step = 50

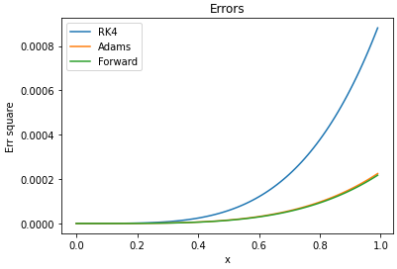

(h) Absolute error of $g(x) = x^3$ with the number of step = 100

Figure 3.1: Polynomial of order 3

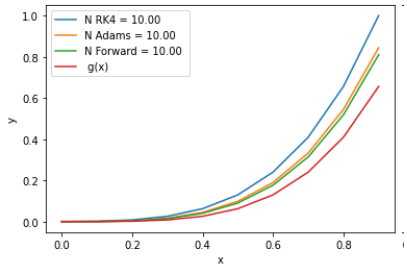

(a) $g(x) = x^4$ with the number of step = 10

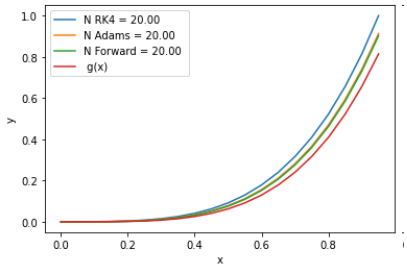

(b) $g(x) = x^4$ with the number of step = 20

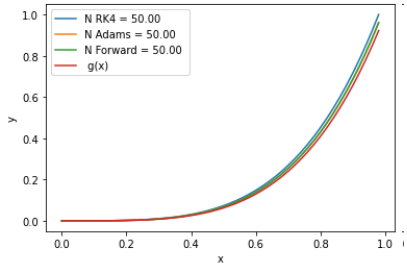

(c) $g(x) = x^4$ with the number of step = 50

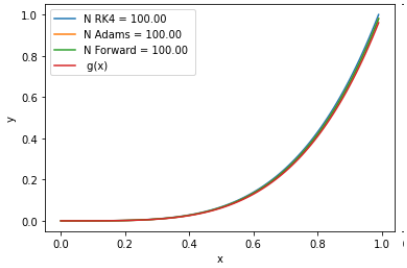

(d) $g(x) = x^4$ with the number of step = 100

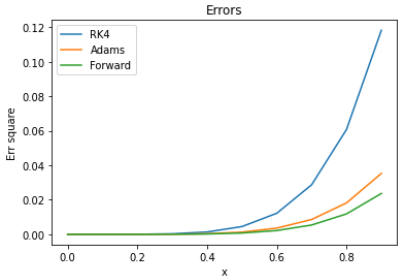

(e) Absolute error of $g(x) = x^4$ with the number of step = 10

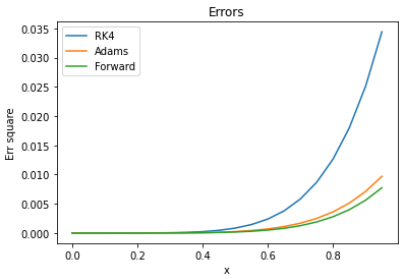

(f) Absolute error of $g(x) = x^4$ with the number of step = 20

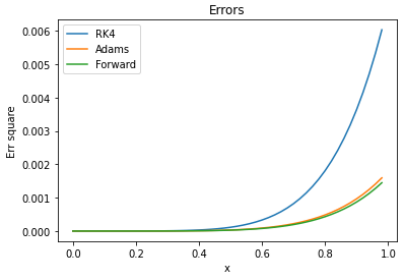

(g) Absolute error of $g(x) = x^4$ with the number of step = 50

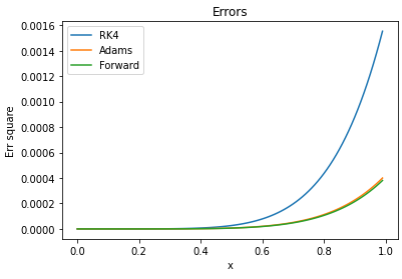

(h) Absolute error of $g(x) = x^4$ with the number of step = 100

Figure 3.2: polynomial of order 4

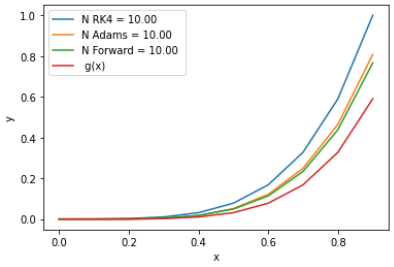

(a) $g(x) = x^5$ with the number of step = 10

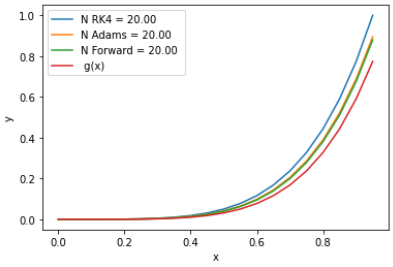

(b) $g(x) = x^5$ with the number of step = 20

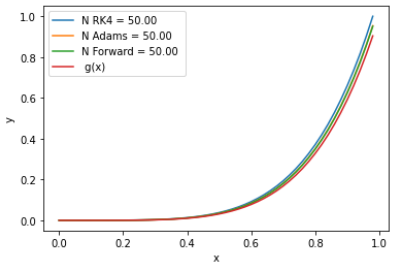

(c) $g(x) = x^5$ with the number of step = 50

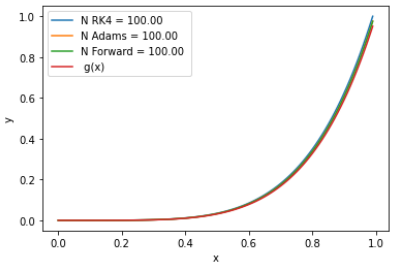

(d) $g(x) = x^5$ with the number of step = 100

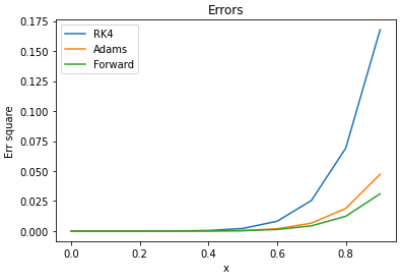

(e) $g(x) = x^5$ with the number of step = 10

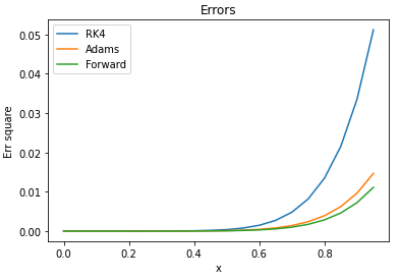

(f) $g(x) = x^5$ with the number of step = 20

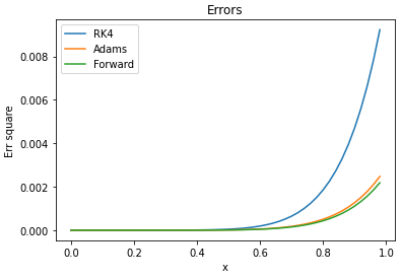

(g) $g(x) = x^5$ with the number of step = 50

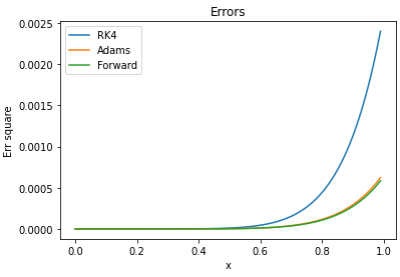

(h) $g(x) = x^5$ with the number of step = 100

Figure 3.3: Polynomial of order 5

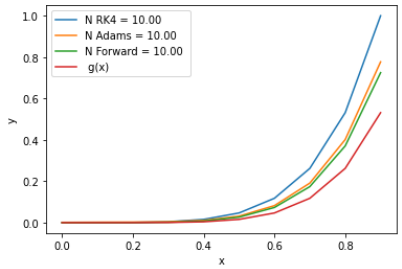

(a) $g(x) = x^6$ with the number of step = 10

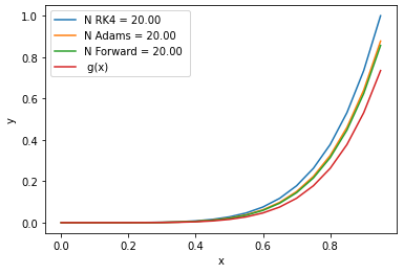

(b) $g(x) = x^6$ with the number of step = 20

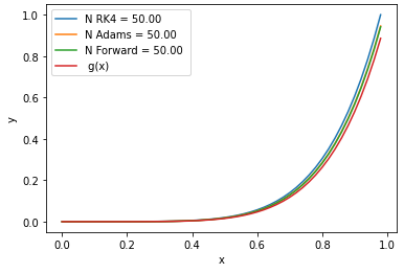

(c) $g(x) = x^6$ with the number of step = 50

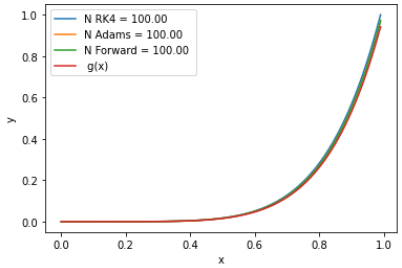

(d) $g(x) = x^6$ with the number of step = 100

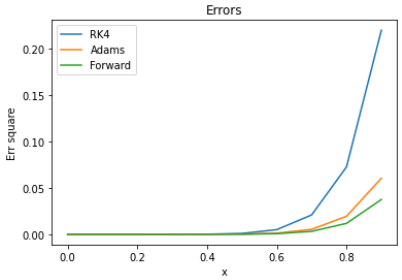

(e) $g(x) = x^6$ with the number of step = 10

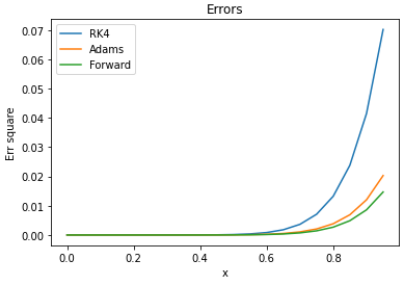

(f) $g(x) = x^6$ with the number of step = 20

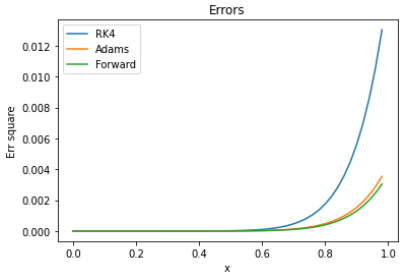

(g) $g(x) = x^6$ with the number of step = 50

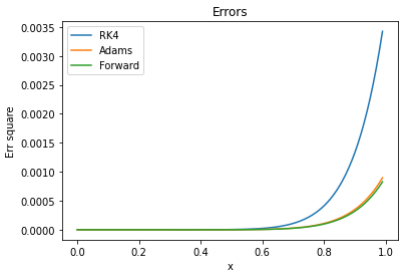

(h) $g(x) = x^6$ with the number of step = 100

Figure 3.4: Polynomial of order 6

The second set of test functions, the sinusoidal shapes and combinations of polynomial shapes and sinusoidal shapes are shown in what follows. Similarly to the polynomials'

case, the four upper panels in each figure, labeled $a-d$ show the numerical evaluations compared to the analytic solution, while the lower panels labeled $e-h$ show the numerical error. The latter shows more varied patterns than in the polynomial case. Summarizing results, one can conclude that for the sin/cos functions and polynomial combinations the Adams and Backward difference methods work better in most cases than RK4, if limited to the interval on $[0, 1]$. We focus on this interval because it is the region of interest for our final study of PDFs and GPDs.

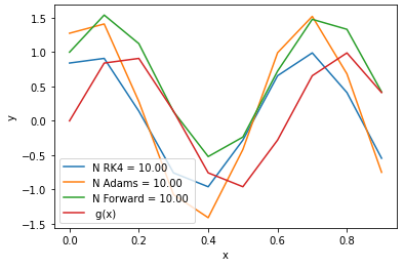

(a) $g(x) = \sin(10x)$ with the number of step = 10

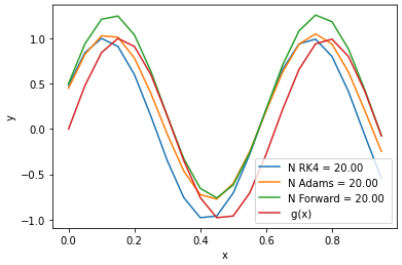

(b) $g(x) = \sin(10x)$ with the number of step = 20

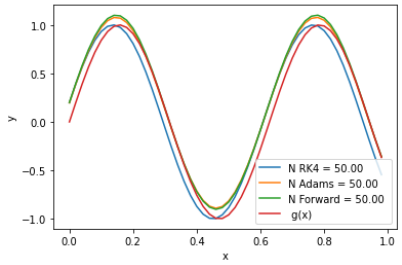

(c) $g(x) = sin(10x)$ with the number of step = 50

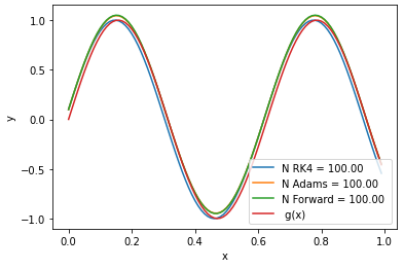

(d) $g(x) = \sin(10x)$ with the number of step = 100

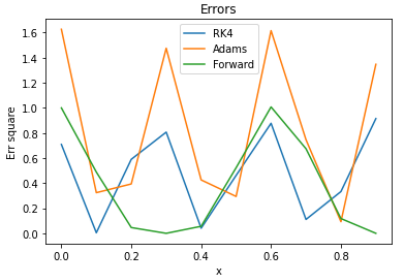

(e) $g(x) = \sin(10x)$ with the number of step = 10

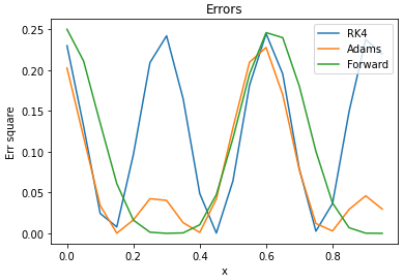

(f) $g(x) = \sin(10x)$ with the number of step = 20

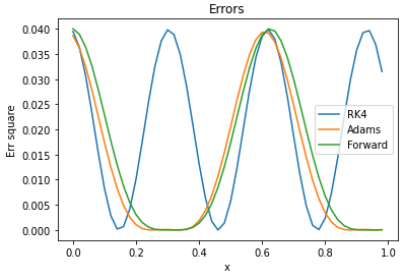

(g) $g(x) = \sin(10x)$ with the number of step = 50

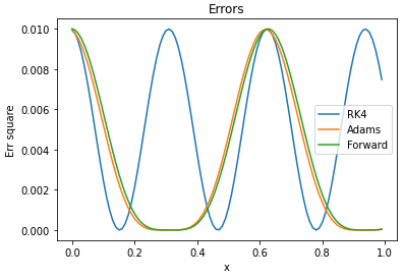

(h) $f(x) = g'(x) = 6x^5$, $g(x) = \sin(10x)$ and $g(x) = \sin(10x)$ with the number of step = 100

Figure 3.5: Sinusoidal functions

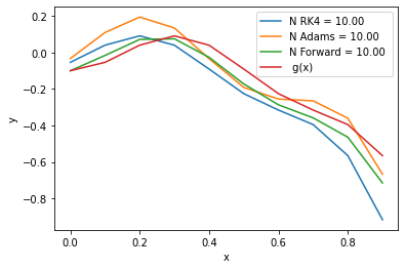

(a) $g(x) = -x^4 - \cos(10x)$ with the number of step = 10

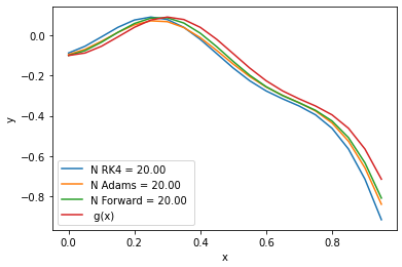

(b) $g(x) = -x^4 - \cos(10x)$ with the number of step = 20

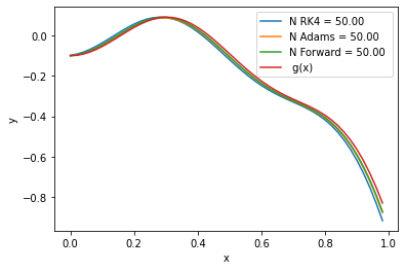

(c) $g(x) = -x^4 - \cos(10x)$ with the number of step = 50

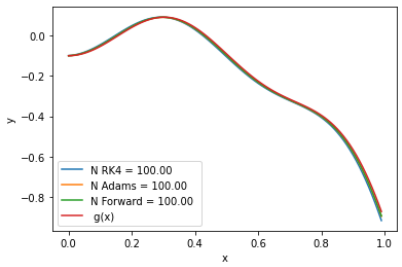

(d) $g(x) = -x^4 - \cos(10x)$ with the number of step = 100

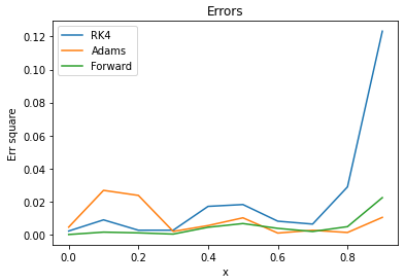

(e) $g(x) = -x^4 - \cos(10x)$ with the number of step = 10

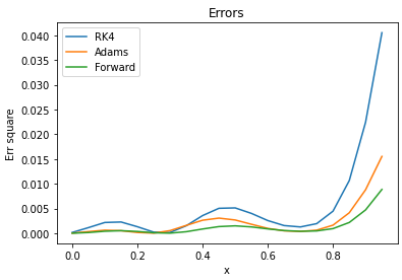

(f) $g(x) = -x^4 - \cos(10x)$ with the number of step = 20

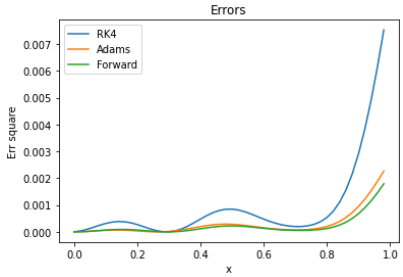

(g) $g(x) = -x^4 - \cos(10x)$ with the number of step = 50

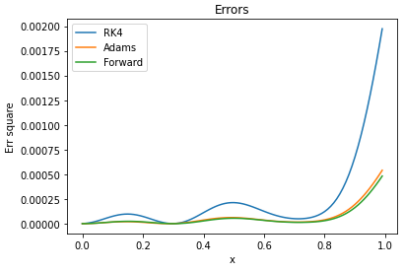

(h) $g(x) = -x^4 - \cos(10x)$ with the number of step = 100

Figure 3.6: Combination of polynomial of order 4 and cos function

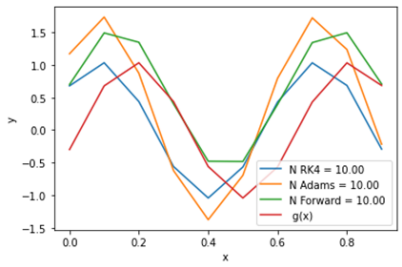

(a) $g(x) = 0.3\cos(10x) + \sin(10x)$ with the number of step = 10

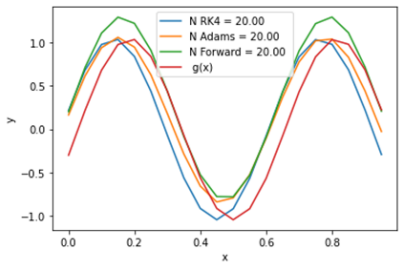

(b) $g(x) = 0.3\cos(10x) + \sin(10x)$ with the number of step = 20

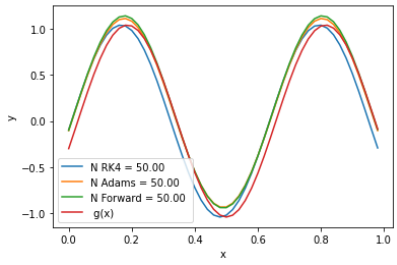

(c) $g(x) = 0.3\cos(10x) + \sin(10x)$ with the number of step = 50

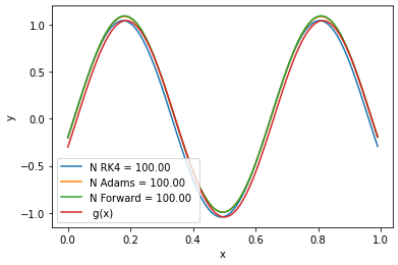

(d) $g(x) = 0.3\cos(10x) + \sin(10x)$ with the number of step = 100

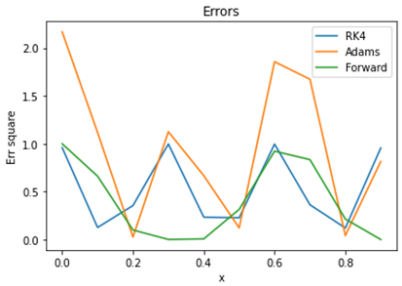

(e) $g(x) = 0.3\cos(10x) + \sin(10x)$ with the number of step = 10

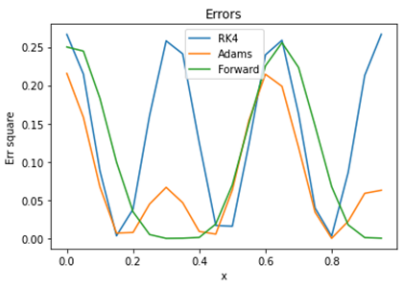

(f) $g(x) = 0.3\cos(10x) + \sin(10x)$ with the number of step = 20

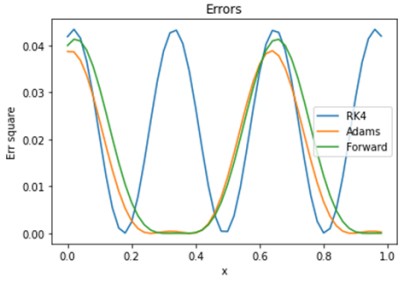

(g) $g(x) = 0.3\cos(10x) + \sin(10x)$ with the number of step = 50

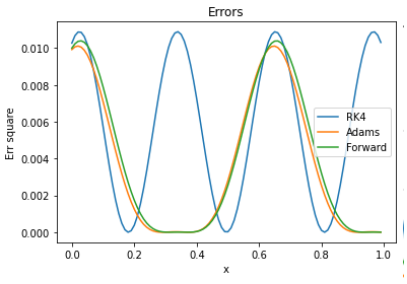

(h) $g(x) = 0.3\cos(10x) + \sin(10x)$ with the number of step = 100

Figure 3.7: Combination of sin and cos function

Finally, results for the exponential and Gaussian functions are presented below with the same labeling scheme as for the previous cases. As one can see from the analysis of the errors' behavior in the lower four panels in each figure, the RK4 method works better for $\exp(-x)$ and Gaussian functions.

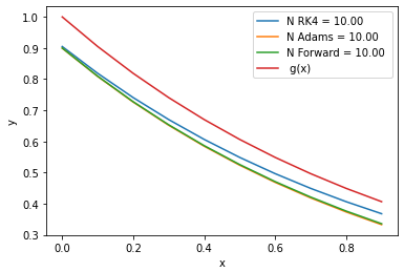

(a) $g(x) = exp(-x)$ with the number of step = 10

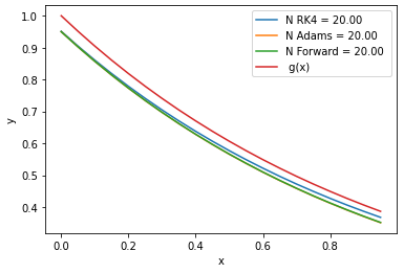

(b) $g(x) = \exp(-x)$ with the number of step = 20

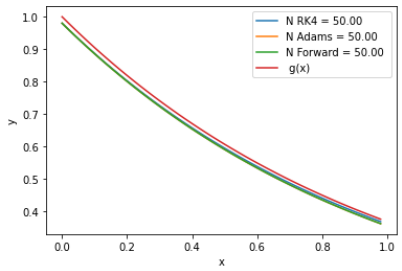

(c) $g(x) = \exp(-x)$ with the number of step = 50

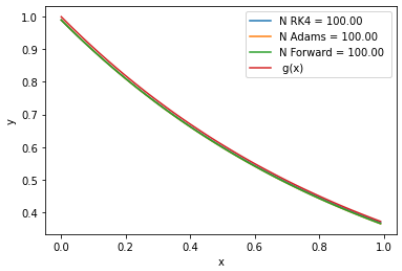

(d) $g(x) = \exp(-x)$ with the number of step = 100

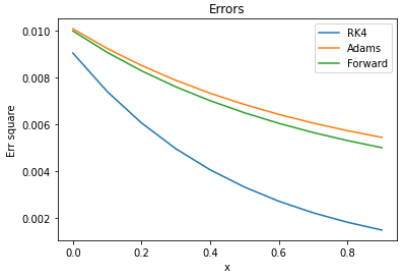

(e) $g(x) = \exp(-x)$ with the number of step = 10

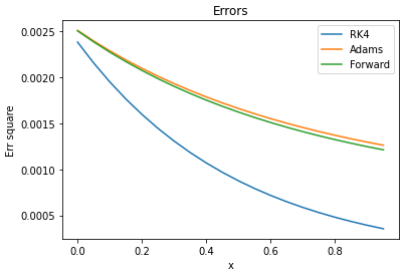

(f) $g(x) = \exp(-x)$ with the number of step = 20

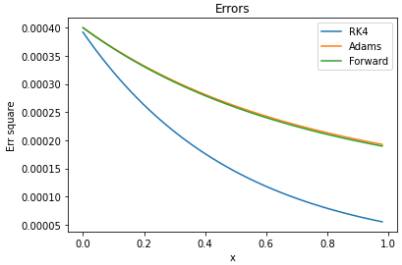

(g) $g(x) = exp(-x)$ with the number of step = 50

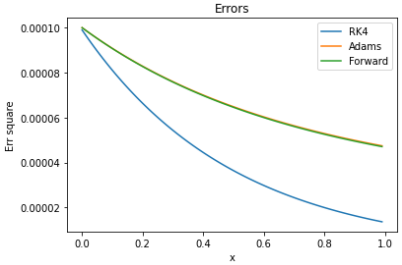

(h) $g(x) = \exp(-x)$ with the number of step = 100

Figure 3.8: $\exp(-x) function$

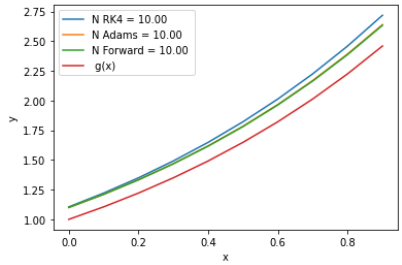

(a) $g(x) = \exp(x)$ with the number of step = 10

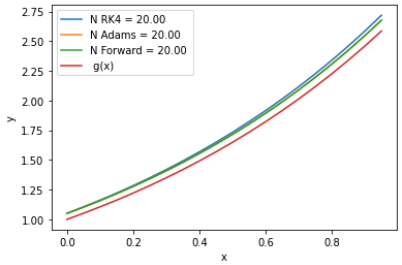

(b) $g(x) = \exp(x)$ with the number of step = 20

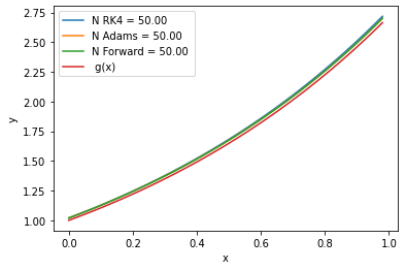

(c) $g(x) = \exp(x)$ with the number of step = 50

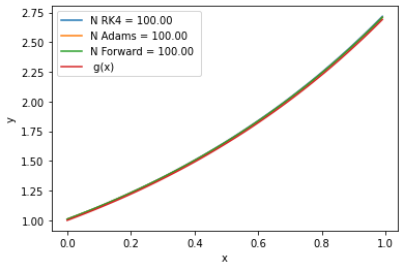

(d) $g(x) = \exp(x)$ with the number of step = 100

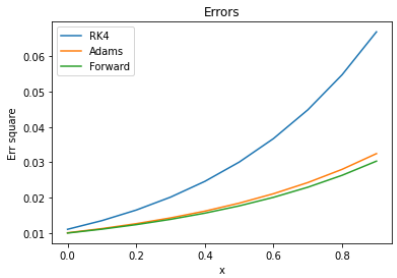

(e) $g(x) = \exp(x)$ with the number of step = 10

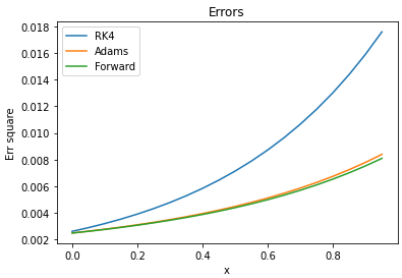

(f) $g(x) = \exp(x)$ with the number of step = 20

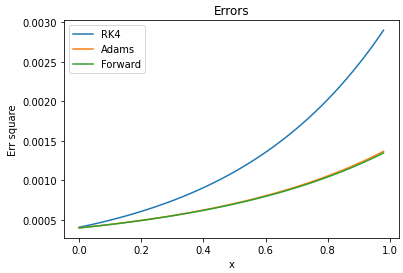

(g) $g(x) = \exp(x)$ with the number of step = 50

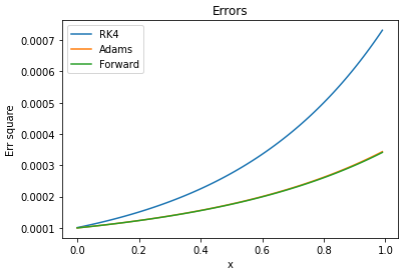

(h) $g(x) = \exp(x)$ with the number of step = 100

Figure 3.9: $\exp(x) function$

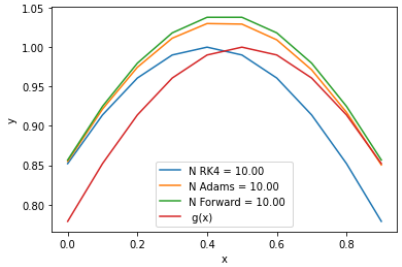

(a) $f(x) = g'(x) = -2x\exp(-x^2)$, g(x)= Gaussian, with the number of step = 10

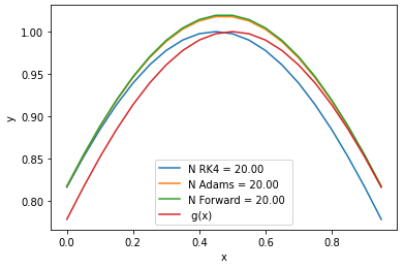

(b) $f(x) = g'(x) = -2x\exp(-x^2)$, g(x)=Gaussian with the number of step = 20

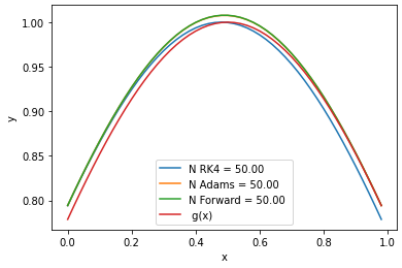

(c) $f(x) = g'(x) = -2x\exp(-x^2)$, g(x)= Gaussian with the number of step = 50

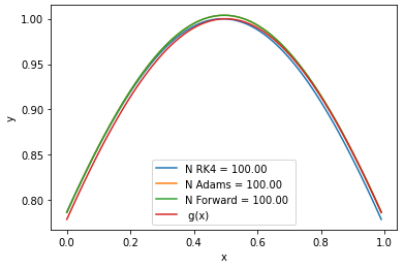

(d) $f(x) = g'(x) = -2x\exp(-x^2)$, g(x)= Gaussian with the number of step = 100

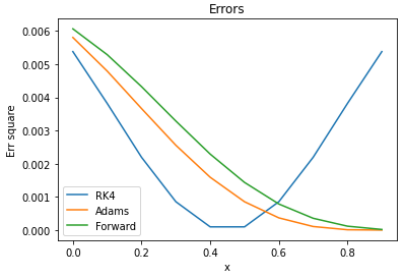

(e) $f(x) = g'(x) = -2x\exp(-x^2)$, g(x)= Gaussian with the number of step = 10

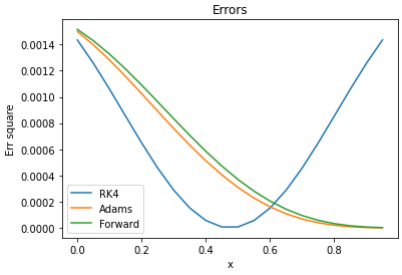

(f) $f(x) = g'(x) = -2x\exp(-x^2)$, g(x)= Gaussian with the number of step = 20

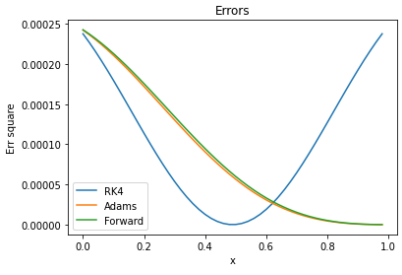

(g) $f(x) = g'(x) = -2x\exp(-x^2)$, g(x)= Gaussian with the number of step = 50

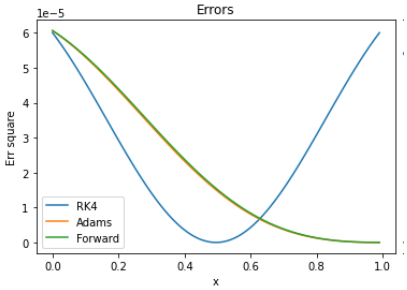

(h) $f(x) = g'(x) = -2x\exp(-x^2)$, g(x)= Gaussian with the number of step = 100

Figure 3.10: Gaussian function

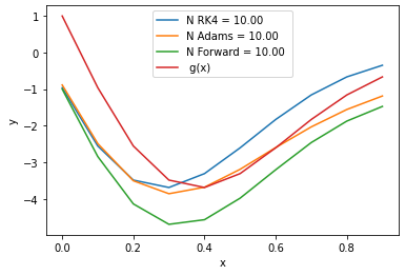

(a) $f(x) = g'(x) = [(1 - 20x)(-8x) - 20]\exp(-4x^2)$, g(x)= derivative of Gaussian with the number of step = 10

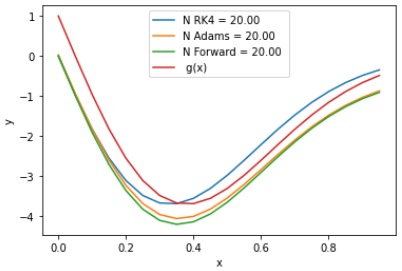

(b) $f(x) = g'(x) = [(1 - 20x)(-8x) - 20]\exp(-4x^2)$, g(x)=derivative of Gaussian with the number of step = 20

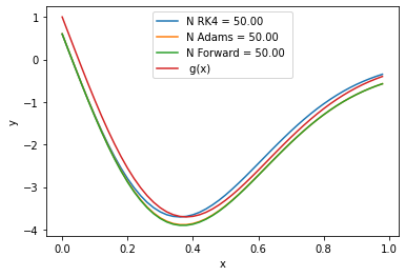

(c) $f(x) = g'(x) = [(1 - 20x)(-8x) - 20]\exp(-4x^2)$, g(x)=derivative of Gaussian with the number of step = 50

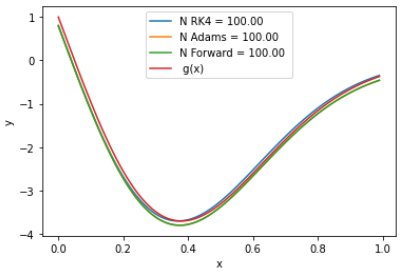

(d) $f(x) = g'(x) = [(1 - 20x)(-8x) - 20]\exp(-4x^2)$, g(x)=derivative of Gaussian with the number of step = 100

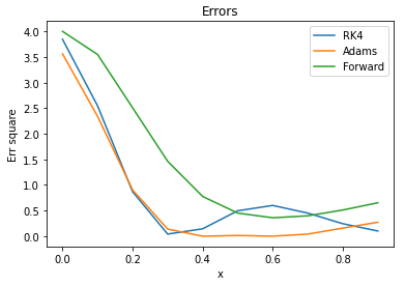

(e) $f(x) = g'(x) = [(1 - 20x)(-8x) - 20]\exp(-4x^2)$, g(x)=derivative of Gaussian with the number of step = 10

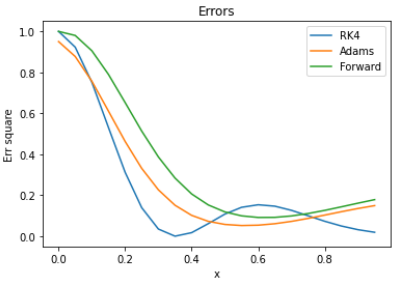

(f) $f(x) = g'(x) = [(1 - 20x)(-8x) - 20]\exp(-4x^2)$, g(x)=derivative of Gaussian with the number of step = 20

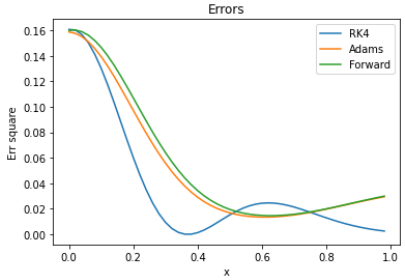

(g) $f(x) = g'(x) = [(1 - 20x)(-8x) - 20]\exp(-4x^2)$, g(x)=derivative of Gaussian with the number of step = 50

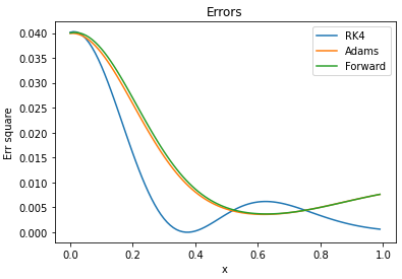

(h) $f(x) = g'(x) = [(1 - 20x)(-8x) - 20]\exp(-4x^2)$, g(x)=derivative of Gaussian with the number of step = 100

Figure 3.11: Derivative Gaussian function

In conclusion, while the Adams method works better with Polynomial, sinusoidal (Periodic) functions and $\exp(x)$, the RK4 method is shown to produce smaller errors for the $\exp(-x)$ and Gaussian shapes. The PDFs, and xPDFs have parametric forms that behave similarly to all of the examples above for x in the interval $[0, 1]$. Since we find no major divergences in the error trend, and actually, sometimes (for polynomials and sinusoidals) a net improvement, the preliminary study presented in this thesis demonstrates that it is justified to use the Adams method for a more efficient and precise evaluation of PQCD Q^2 evolution.

Chapter 4

Procedure Checklist

There is a lot of complexity involved in the QCD evolution equations program. In what follows, I would illustrate the various processes addressed in this thesis project with the goal of producing a product that is useful for anyone that would like to run the evolution equations and faithfully reproduce results according to a well defined set of steps and benchmarks.

The DGLAP equation mentioned earlier, is shown again here,

$$\frac{dF^{NS}(x,Q^2)}{d\ln Q^2} = C_F\frac{\alpha_s}{2\pi}\Bigg\{\int_x^1 \frac{dz}{1-z}\Big[(1+z^2)F^{NS}\big(\frac{x}{z},Q^2\big) - 2F^{NS}\big(x,Q^2\big)\Big] + \Big[\frac{3}{2}+2\ln(1-x)\Big]F^{NS}\big(x,Q^2\big)\Bigg\} \tag{4.1}$$

The variables which I use in the numerical calculation are x and y. Therefore, let's transform Eq.(4.1) in terms of x and y,

$$\frac{dF^{NS}(x,Q^2)}{d^2} = C_F\frac{\alpha_s}{2\pi}\Bigg\{\int_x^1 \frac{xdy}{y^2\left[1-\left(\frac{x}{y}\right)^2\right]}\Bigg\{\left[1+\left(\frac{x}{y}\right)^2\right]F^{NS}\big(y,Q^2\big) - 2F^{NS}\big(x,Q^2\big)\Bigg\} + \Big[\frac{3}{2}+2\ln(1-x)\Big]F^{NS}\big(x,Q^2\big)\Bigg\} \tag{4.2}$$

4.1 x-y Spacing

The first step is to construct x and y space as we can see clearly that whole Eq.(4.2) could be computed just only using x and y as building blocks.

How would the x and y be built? The key involves with the initial xPDFs which we used in our work.

The initial conditions have been set up at the Les Houches meeting (reference). The initial energy is at

$$Q_0^2 = 2\text{GeV}^2 \tag{4.3}$$

The initial distributions are from CTEQ5M parametrization. The distributions are

$$\begin{aligned}
xu_v(x,{Q_0}^2) &= 5.107200x^{0.8}(1-x)^3 && (4.4)\\
xd_v(x,{Q_0}^2) &= 3.064320x^{0.8}(1-x)^4 && (4.5)\\
xg(x,{Q_0}^2) &= 1.700000x^{-0.1}(1-x)^5 && (4.6)\\
x\overline{d}(x,{Q_0}^2) &= 0.1939875x^{-0.1}(1-x)^6 && (4.7)\\
x\overline{u}(x,{Q_0}^2) &= (1-x)xd_v(x,{Q_0}^2) && (4.8)\\
xs(x,{Q_0}^2) &= x\overline{s}(x,{Q_0}^2) = 0.2x(\overline{u}+\overline{d})(x,{Q_0}^2) && (4.9)
\end{aligned}$$

Let's look at the following figure thoroughly. The figure is our used initial xPDFs of a proton (Eqs.(4.4) to (4.9).

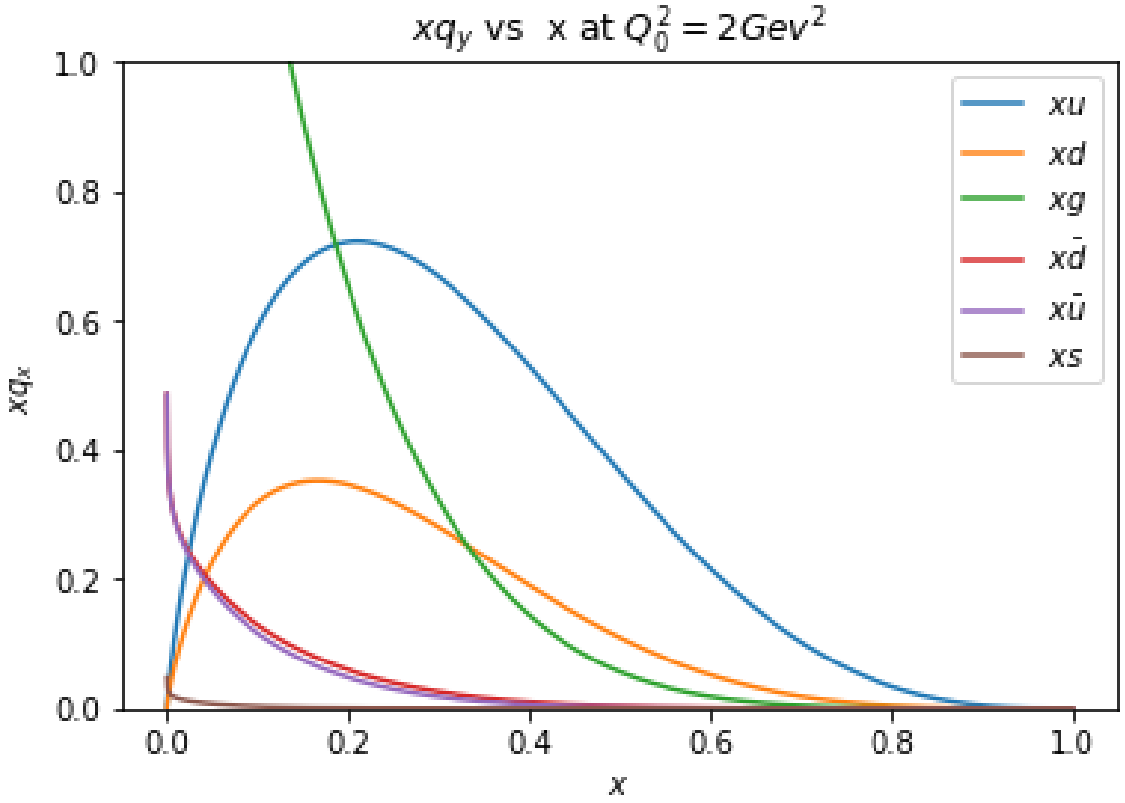

Figure 4.1: Distribution of all xPDFs

The behaviors of any xPDF can be clustered into an exponential decay and a Log-normal distribution.

As you can see from the graph, xPDFs of up and down quarks are the Log-normal distribution corresponding to the conservation of up and down quarks. In the opposition, the xPDFs of gluon, other quarks and anti-quarks behave like the exponential decay curve according to zero conservation rules.

This is the reason why there must be a specific way to do a spacing of x and y. I did both linear spacing and exponential spacing of x and y.

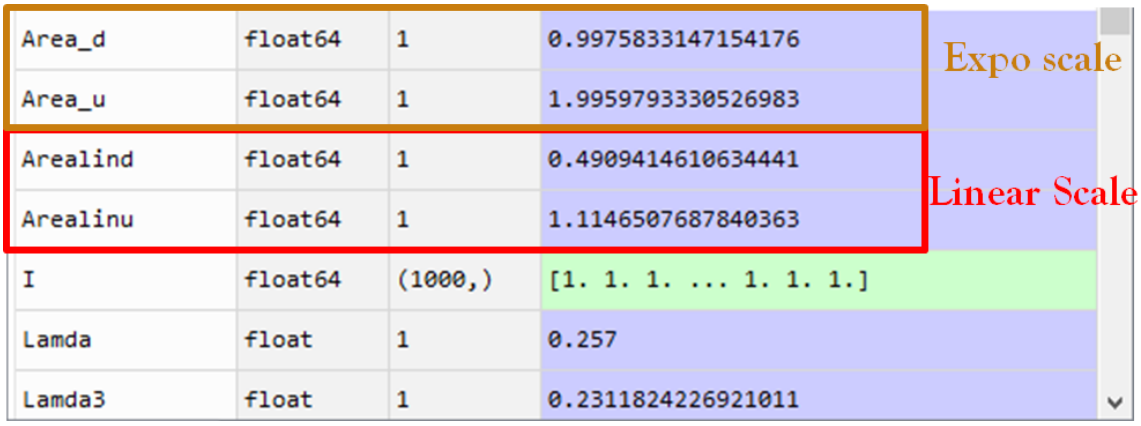

Figure 4.2: Linear Vs exponential spacing

To illustrate the importance of spacing of x and y, I did both linear and exponential technique as I mentioned earlier and did a calculation of a total number of up and down quarks.

The conservation number of up and down quarks for a proton are 2 and 1 in order. With the same number of elements in a range of $x, y = 0$ to $x, y = 1$, the exponential spacing works better than the linear spacing.

As a result, the exponential spacing was used in this project. The spacing of x and y would be shown in the following graph.

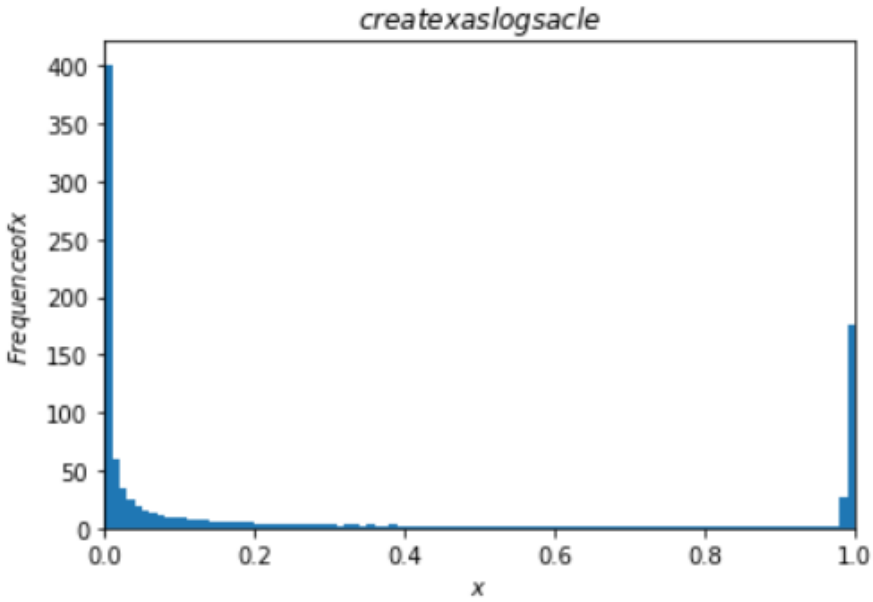

Figure 4.3: Distribution of x-space

The distribution of x in this work is the exponential decay at the first 800 elements and distribute as a linear at the rest.

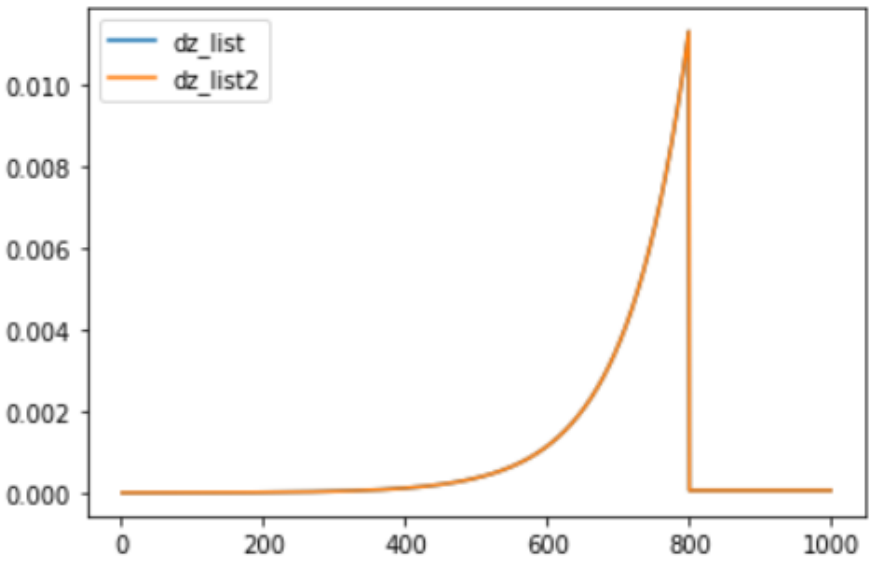

Figure 4.4: Difference of x-space

or the exponential distribution can be shown by a difference of x in the interval [0,1] as in the figure 4.4 above.

We believe the reason why exponential x-spacing works better because the exponential curve behave more similarly to the initial xPDF than a linear scale. Maybe other better spacing types would be found in the future, but this one works efficiently for now.

4.2 Evaluation of the Running Coupling constant(α_s)

The basic knowledge of this section can be found in chapter 2 of Ref.Roberts 1990.

α_s is defined as,

$$\alpha_s(Q^2) = \frac{4\pi}{\beta_0 \ln(Q^2/\Lambda^2)}, \tag{4.10}$$

where,

$$\beta_0 = 11 - \frac{2}{3}N_f. \tag{4.11}$$

As we remember from chapter 2, the running constant changes with the value of Q^2. When the number of flavors, $N_f = 3$, $Q^2 \leq {m_c}^2$, m_c being the mass of the charmed quark, c; when $N_f = 4$, ${m_c}^2 \leq Q^2 \leq {m_b}^2$, m_b being the mass of the b quark; lastly, when ${m_b}^2 \leq Q^2$, $N_f = 5$.

The corresponding corrections to the Λ parameter $\Lambda \Rightarrow \Lambda_{(N_f)}$, which can be described with the set of following equations with varying number of flavors, N_f,

$$\Lambda_{(3)} = \Lambda_{(4)}\left(\frac{m_c}{\Lambda_{(4)}}\right)^{\frac{2}{27}} \tag{4.12}$$

$$\Lambda_{(5)} = \Lambda_{(4)}\left(\frac{m_b}{\Lambda_{(4)}}\right)^{-\frac{2}{23}} \tag{4.13}$$

Where $\Lambda_{(4)} \approx 200$ MeV for a proton, $m_{(c)} = 2\ GeV^2$, $m_{(b)} = 4.5\ GeV^2$, and $m_{(t)} = 175\ GeV^2$

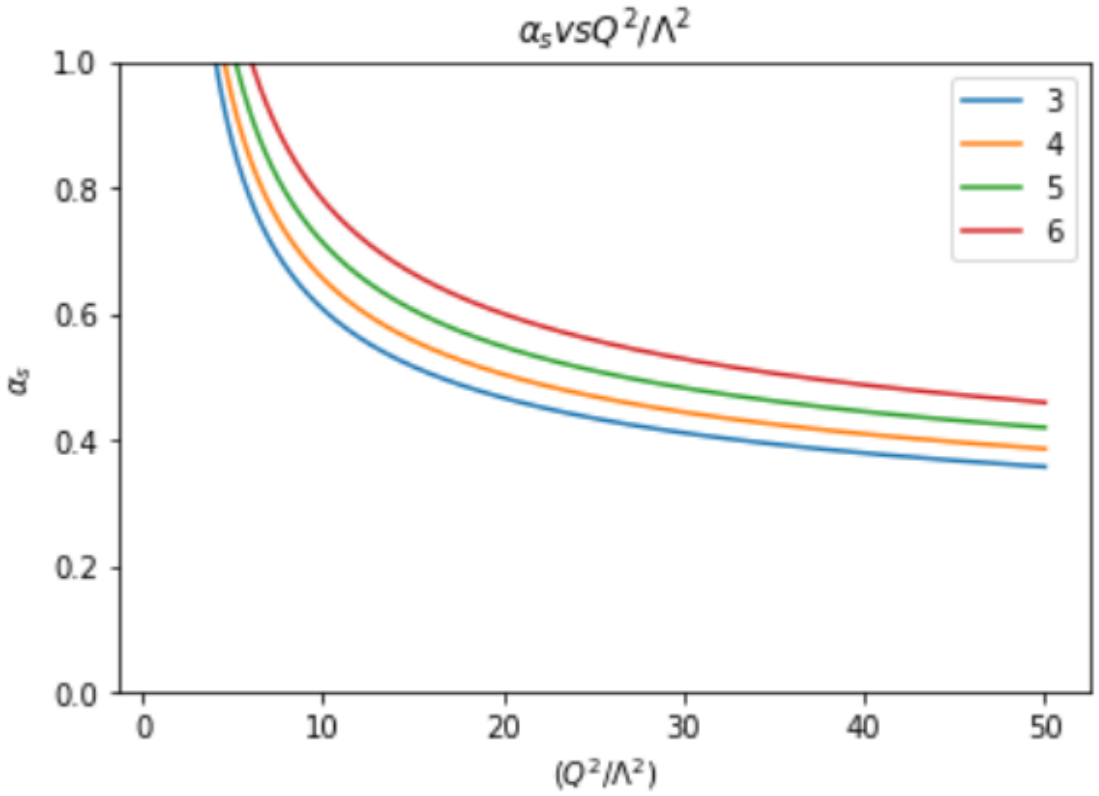

Figure 4.5: α_s without the correction of Λ

These curves show the running coupling constant without using the correction of Λ. You can see that will be a discontinuous connection among $N_f = 3, 4, 5, 6$ while the Q^2 is increasing.

The discontinuity could be more smoother using the correction which we mentioned above. The following graph using the correction and the discontinuity was disappeared. This graph show $N_f = 3, 4, 5$, ${m_c}^2$(blue dot) and ${m_b}^2$(orange dot)

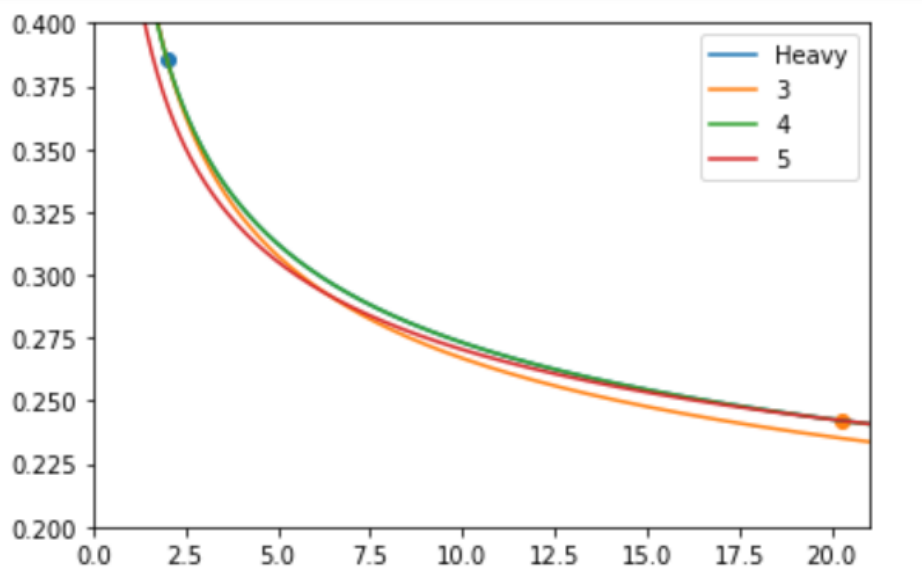

Figure 4.6: α_s with the correction of Λ

And then, I keep only the intersected α_s related with the condition of N_f and Q^2. Finally, this blue curve in a figure 4.7is the running coupling which was used in this project.

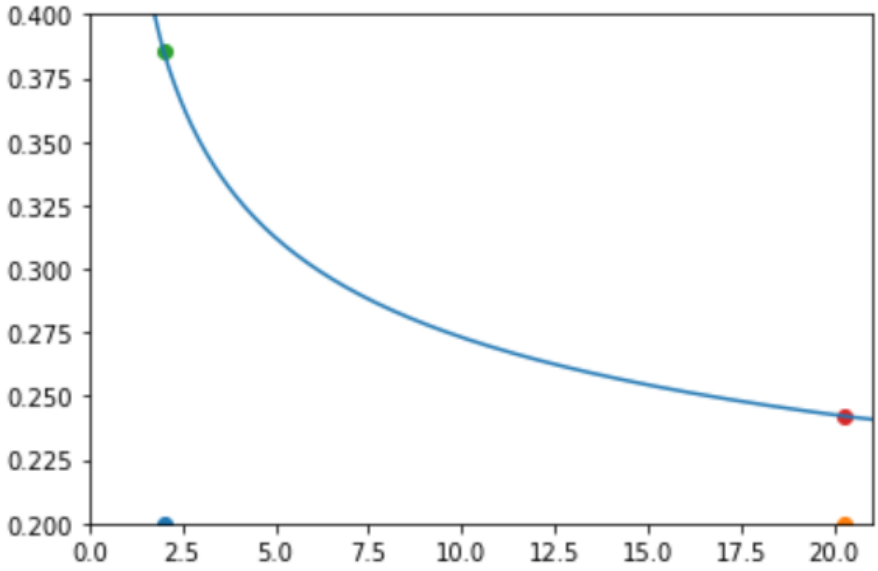

Figure 4.7: α_s with the correction of Λ which we used

4.3 Derivative of the Structure Function

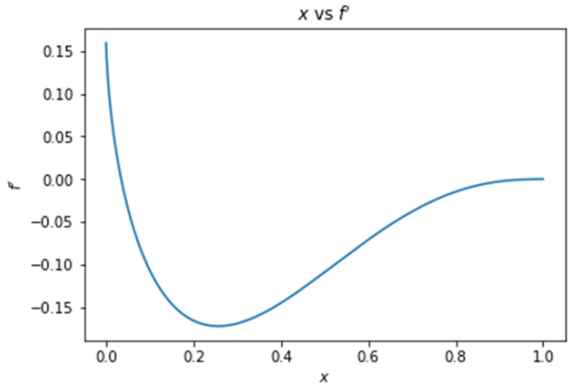

(a) Produced derivative of xPDF of an up quark

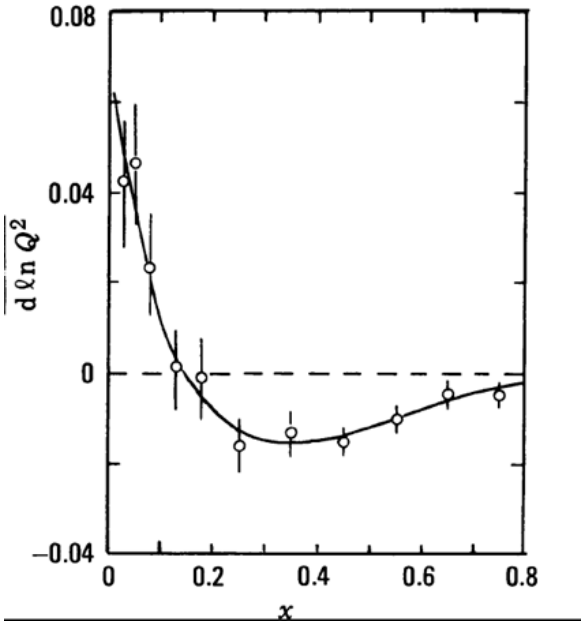

(b) A derivative of structure function F_2 measured in moun-proton scattering by EMC(Aubert et al.1986). The curve corresponds to a leading order with $\Lambda = 90$ MeV in [Roberts 1990]

Figure 4.8: Derivative of a structure function

These figures show the similar behavior of a derivative of the structure function and XPDFs. The checklist idea is about there are 2 parts beyond and under the zero line. In my experience, the graph will be only at the upside or downside, if there are something wrong with the DGLAP formula for a Non-singlet case.

Therefore, the produced derivative of xPDFs should corresponds to the derivative of the structure function F_2 above.

4.4 Sum Rules

There are several conservation rules.

$$\int_0^1 dz P_{qq}(z) = 0$$
$$\int_0^1 dz u_v(x) = 2 \tag{4.14}$$

The meaning of the second rule is summing over all of the xPDF of an up valence quark give the total number of up quarks inside the proton which is 2.

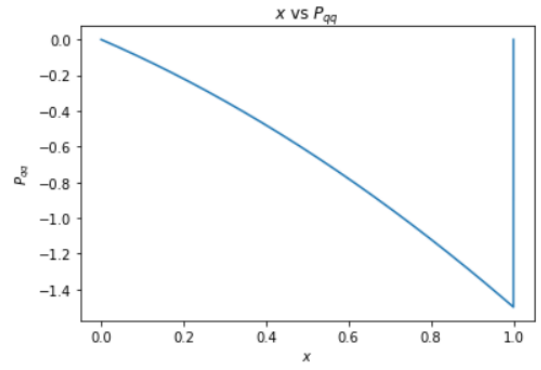

(a) P_{qq} sum rule

```
Total number of u quark of  76 th loop is  1.9985683402921952
Total number of u quark of  77 th loop is  1.9985981786559375
Total number of u quark of  78 th loop is  1.9986279129187068
Total number of u quark of  79 th loop is  1.998657542807308
Total number of u quark of  80 th loop is  1.9986870680482718
Total number of u quark of  81 th loop is  1.998716488367875
Total number of u quark of  82 th loop is  1.9987458034921326
Total number of u quark of  83 th loop is  1.9987750131468018
Total number of u quark of  84 th loop is  1.998804117057377
Total number of u quark of  85 th loop is  1.998833114949098
Total number of u quark of  86 th loop is  1.9988620065469516
Total number of u quark of  87 th loop is  1.99889079157566
Total number of u quark of  88 th loop is  1.9989194697596975
Total number of u quark of  89 th loop is  1.998948040823284
Total number of u quark of  90 th loop is  1.9989765044903867
Total number of u quark of  91 th loop is  1.999004860484713
Total number of u quark of  92 th loop is  1.9990331085297295
Total number of u quark of  93 th loop is  1.9990612483486483
Total number of u quark of  94 th loop is  1.9990892796644293
Total number of u quark of  95 th loop is  1.999117202199787
Total number of u quark of  96 th loop is  1.9991450156771846
Total number of u quark of  97 th loop is  1.9991727198188378
Total number of u quark of  98 th loop is  1.9992003143467214
Total number of u quark of  99 th loop is  1.9992277989825604
```

(b) u_v sum rule

Figure 4.9: Sum rules

The figure on the left is a graph of x vs a summation of x going from x=0 to x=1. It shows to 1^{st} sum rule is valid in our work.

The next one is showing the conservation of the sum rule of u_v. The total number of up valence quark must be always extremely close to 2, even we make a very high final energy level or extremely high number of step in the calculation. For here, I show a 100 number of steps and it still conserve.

$$\int_0^1 dzz[P_{qq}(z) + P_{Gq}(z)] = 0$$
$$\int_0^1 dzz[2N_f P_{qG}(z) + P_{GG}(z)] = 0 \tag{4.15}$$

These 2 equations mean the momentum conservation of a parent quark and gluon in order.

Here again, I attached the best picture to describe the momentum conservation of the parent quark and gluon[R.Field]

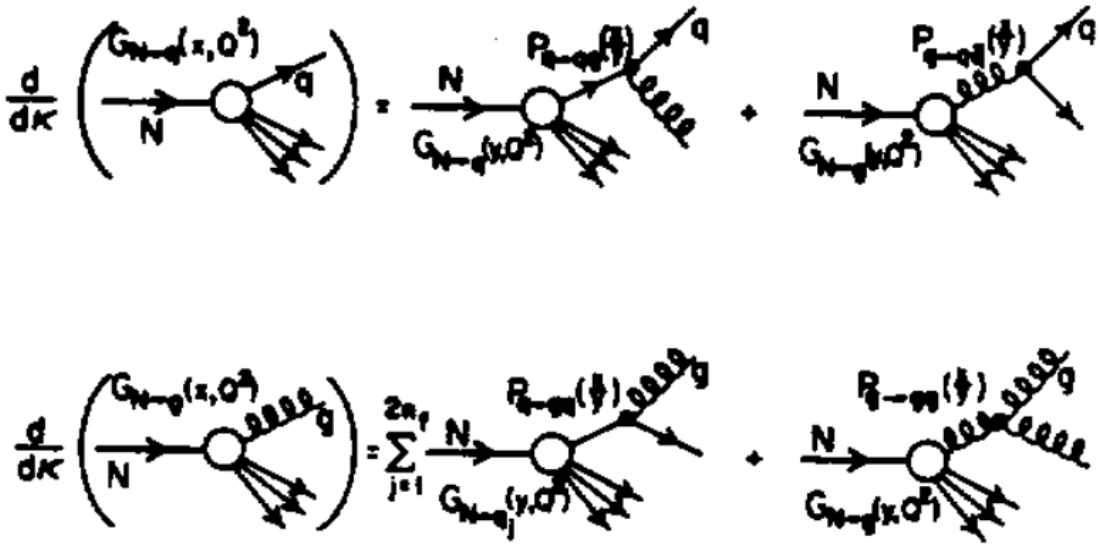

Figure 4.10: Splitting function and their parent quark and gluon [Field and Pines 1995]

The vertexes on the upper right of the Feynman diagrams show the illustration of splitting functions. The 2 upper diagrams show the combination of getting the final quark from quark and produces gluon as (P_{qg}) and from gluon and produces another quark as (P_{qq}).

others also show the combination of getting the final gluon from quark and produces quark as (P_{gq}) and from gluon and produces another gluon as (P_{gg}).

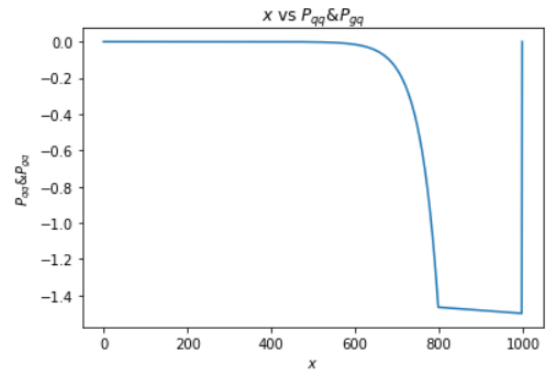

(a) P_{qq} and P_{Gq} sum rule

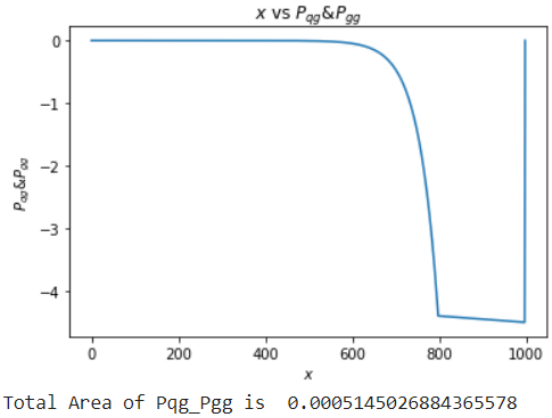

(b) P_{qG} and P_{GG} sum rule

Figure 4.11: Momentum sum rules

Hence, these are the results were produced to confirm the analytic results. The left-hand side show the x' element vs the sum rule of the parent quark on from x'=0 to x'=x. Similarly, the right-hand side show the x' element vs the sum rule of the parent gluon on from x'=0 to x'=x.

Moreover, the evolution results still show the validity of the sum rules by the following graphs.

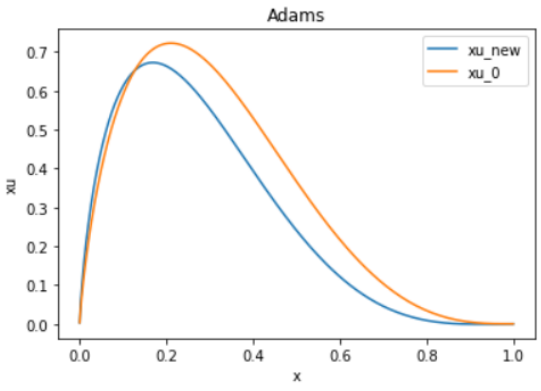

(a) The evolution of xu_v from $Q^2 = 2GeV^2$ to $Q^2 = 10GeV^2$

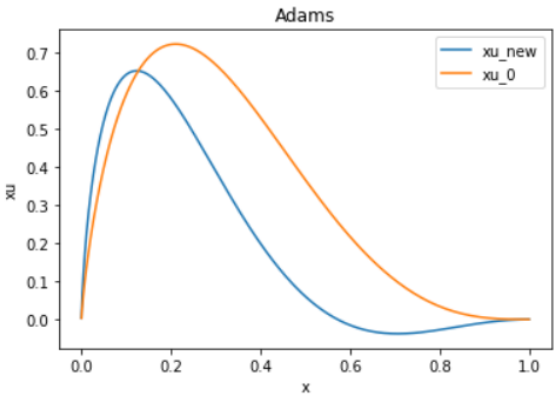

(b) The evolution of xu_v from $Q^2 = 2GeV^2$ to $Q^2 = 100GeV^2$

Figure 4.12: Evolutions to $Q^2 = 10GeV^2$ and $Q^2 = 100GeV^2$

The blue line is the initial xPDF and the orange line is the final xPDF in the evolution process.

The evolution from initial energy level 2 GeV^2 to the energy level 10 GeV^2 was shown on the left and the evolution from initial energy level 2 GeV^2 to the energy level 100 GeV^2 was shown on the right. These graphs show decreasing on the right-region and increasing on the left-region. As we know about the Bjorken, the maximum distribution point will go to x=0 as Q^2 go to ∞

And the all above results confirm that the sum rules are valid in our work.

4.5 Mellin Moment

As the equations in the Mellin Moment in Chapter1, we can used those equations and get the relation of ${M_n}^{-1/d_n}$ and lnQ^2 as

$$ {M_n}^{NS}(Q^2) = {M_n}^{NS}({Q_0}^2)\left[\frac{\alpha_s(Q^2)}{\alpha_s({Q_0}^2)}\right]^{d_n^{NS}} \tag{4.16} $$

and

$$ \alpha_s(Q^2) = \frac{4\pi}{\beta_0 ln\big(Q^2/\Lambda^2\big)} \tag{4.17} $$

Let substitue eq.(4.17) into eq. (4.16) and rearrange into

$$ \frac{{M_n}^{NS}(Q^2)}{{M_n}^{NS}({Q_0}^2)} = \left[\frac{4\pi}{\alpha_s({Q_0}^2)\beta_0 ln\big(Q^2/\Lambda^2\big)}\right]^{d_n^{NS}} \tag{4.18} $$

$$ \left[\frac{{M_n}^{NS}(Q^2)}{{M_n}^{NS}({Q_0}^2)}\right]^{1/d_n^{NS}} = \frac{4\pi}{\alpha_s({Q_0}^2)\beta_0 ln\big(Q^2/\Lambda^2\big)} \tag{4.19} $$

$$\left[{M_n}^{NS}(Q^2)\right]^{-1/d_n^{NS}} = \frac{\alpha_s({Q_0}^2)\beta_0}{4\pi[{M_n}^{NS}({Q_0}^2)]^{1/d_n^{NS}}} ln\big(Q^2/\Lambda^2\big) \tag{4.20}$$

$$\left[{M_n}^{NS}(Q^2)\right]^{-1/d_n^{NS}} = \frac{\alpha_s({Q_0}^2)\beta_0}{4\pi[{M_n}^{NS}({Q_0}^2)]^{1/d_n^{NS}}} \left[ln\big(Q^2\big) - ln\big(\Lambda^2\big)\right] \tag{4.21}$$

Lastly, the equation shows the linearity of ${M_n}^{-1/d_n}$ and lnQ^2. According to the equation above, the numerical results were produced in the similar way to the results of muon and neutrino data provided in [Robert]. The calculated orders of Mellin moment start from n=3 to n=8.

To calculate the NS Mellin moment of each order, the table of constants of asymptotic freedom for $N_f = 4$ (Gross-Wilczek convention)

n	${d_n}^{qq}$
3	0.6667
4	0.8373
5	0.9707
6	1.0804
7	1.1737
8	1.2550

Table 4.1: Constants of asymptotic freedom for $N_f = 4$ (Gross-Wilczek convention) [Roberts 1990]

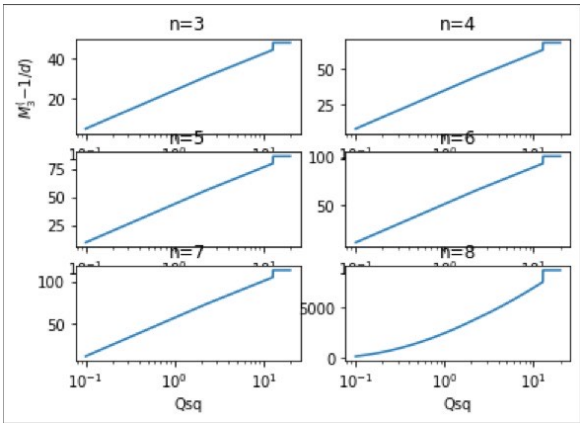

(a) Our computed ${M_n}^{NS}$ to the power $-1/d_n^{NS}$ against lnQ^2

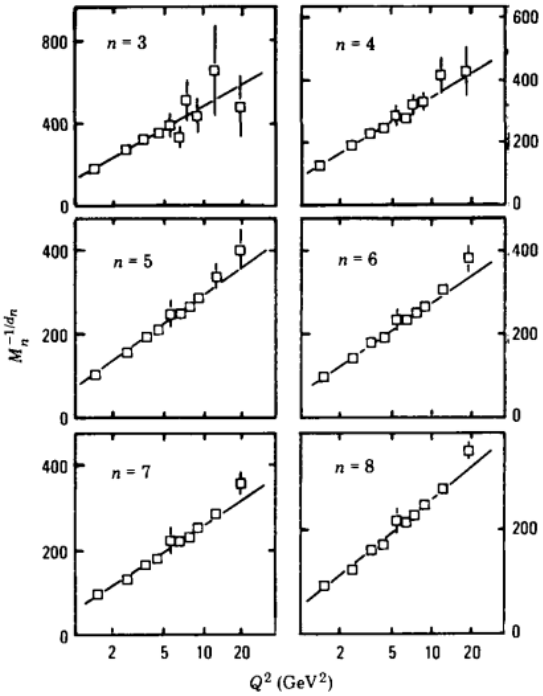

(b) Non-singlet moments ${M_n}^{NS}$ computed from muon and neutrino data, to the power $-1/d_n^{NS}$ against lnQ^2 [Roberts 1990]

Figure 4.13: Calculated a linear character of Mellin moments

As a result, the results were produced to confirm the analytic results of the linearity of the Mellin moment. The left-hand side show the linear curves of computed Mellin moments from n=3 to n=8 and they behave like we expected. Similarly, the right-hand side is the real data illustrates the linearity of the Mellin moment from muon and neutrino[Roberts 1990].

And the 2 results above confirm the correct behavior of Mellin moment with the energy level.

Chapter 5

Results

The main results which I would like to present are the variation of the number of step(N) and the final energy scale(Q^2) of all 3 methods. Then, the comparison of error percentages(%) and time(s) are shown in the following graphs.

The variation of N is a list of N=[1,2,3,4,5] and the variations of Q^2 is a list of Q^2 =[10,20,50,100,200,500,1000].

Where time is measured by the help of library namely time in Python.

I analyze and show the data into 6 topics which are number of steps vs error(%) of all methods at each energy level, number of steps vs time(s) of all methods at each energy level, Q^2 vs error(%) of all methods at each number of steps, Q^2 vs time(s) of all methods at each number of step, number of steps vs error(%) of all Q^2 of each method, number of steps vs time(s) of all Q^2 of each method, and DGLAP Evolution Limit using the GPD Evolution Equation.

5.1 Number of Steps Vs Error of all Methods at Each Energy Level

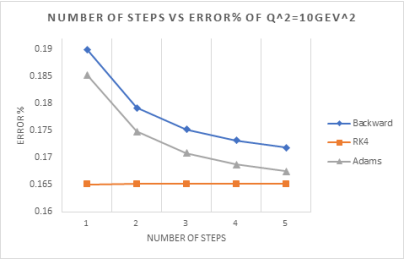

(a) N vs Error percentage of $Q^2 = 10GeV^2$

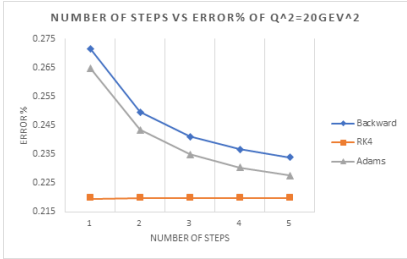

(b) N vs Error percentage of $Q^2 = 20GeV^2$

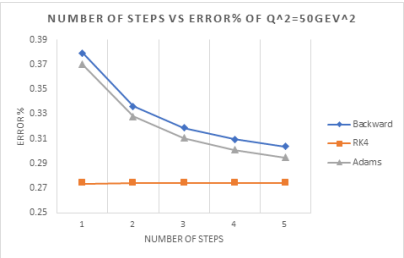

(c) N vs Error percentage of $Q^2 = 50GeV^2$

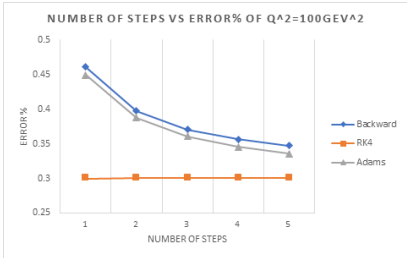

(d) N vs Error percentage of $Q^2 = 100GeV^2$

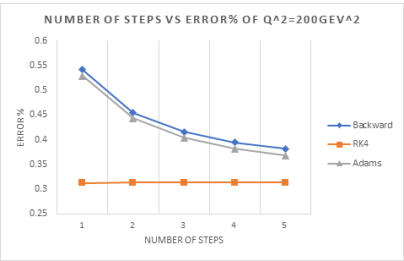

(e) N vs Error percentage of $Q^2 = 200GeV^2$

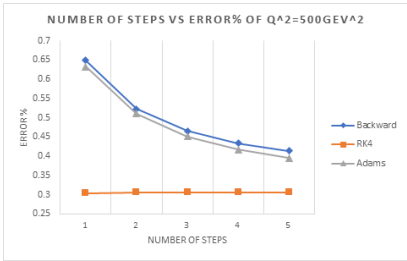

(f) N vs Error percentage of $Q^2 = 500GeV^2$

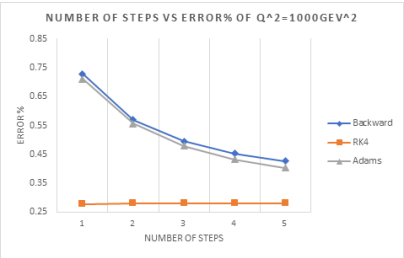

(g) N vs Error percentage of $Q^2 = 1000GeV^2$

Figure 5.1: Number of Steps Vs Error of all Methods at Each Energy Level

5.2 Number of Steps Vs Time of all Methods at Each Energy Level

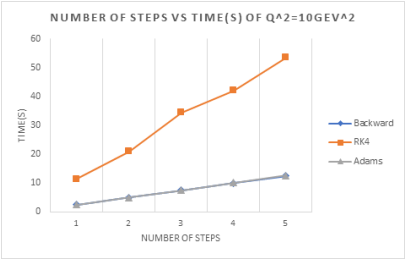

(a) N vs Time(s) of $Q^2 = 10GeV^2$

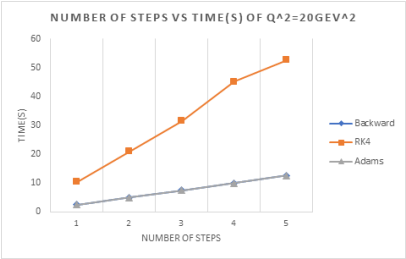

(b) N vs Time(s) of $Q^2 = 20GeV^2$

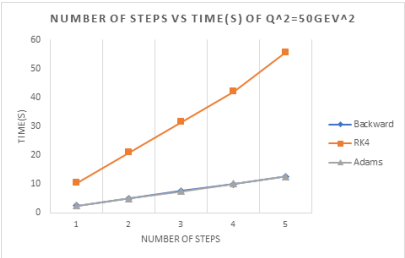

(c) N vs Time(s) of $Q^2 = 50GeV^2$

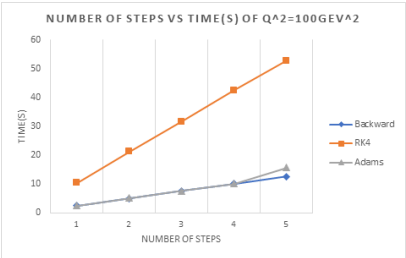

(d) N vs Time(s) of $Q^2 = 100GeV^2$

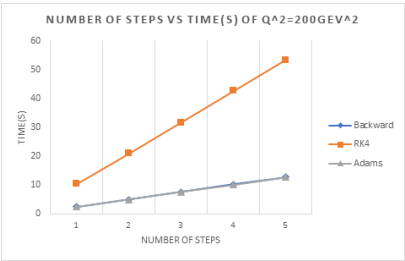

(e) N vs Time(s) of $Q^2 = 200GeV^2$

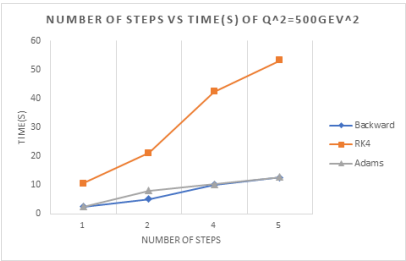

(f) N vs Time(s) of $Q^2 = 500GeV^2$

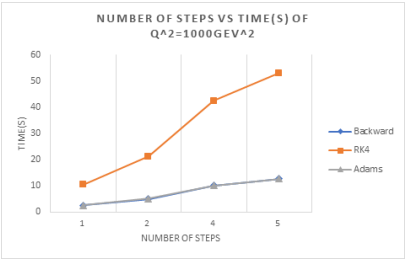

(g) N vs Time(s) of $Q^2 = 1000GeV^2$

Figure 5.2: Number of Steps Vs Time of all Methods at Each Energy Level

5.3 Q^2 Vs Error of all Methods at Each Number of Steps

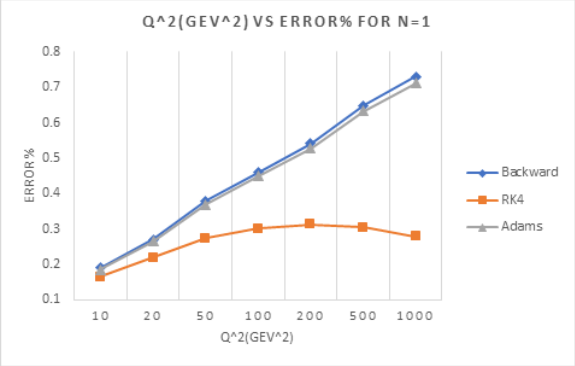

(a) Q^2 vs Error percentage of N=1

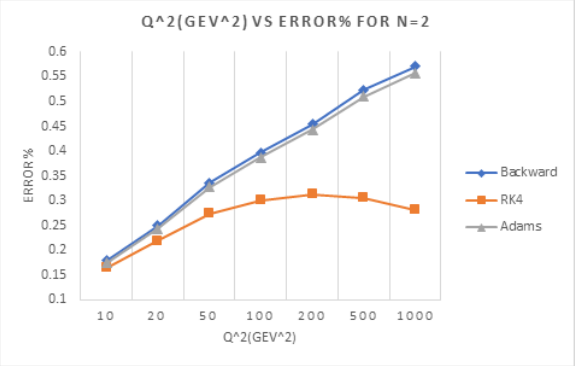

(b) Q^2 vs Error percentage of N=2

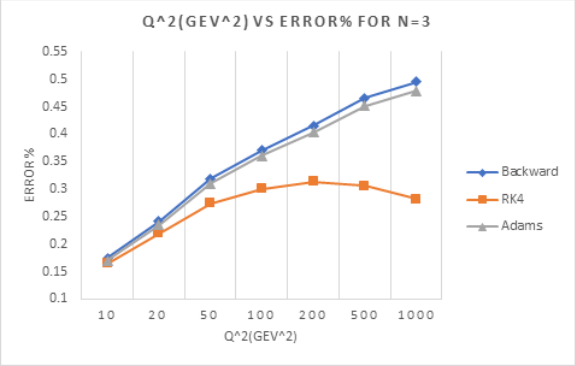

(c) Q^2 vs Error percentage of N=3

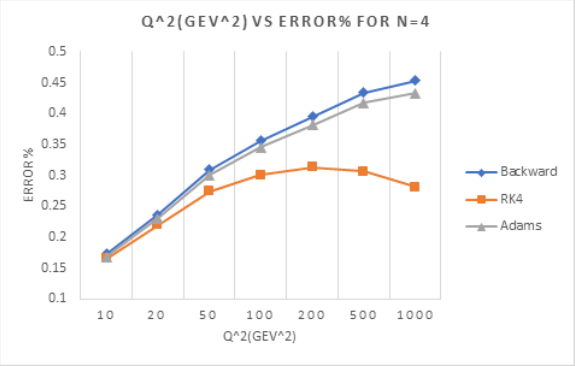

(d) Q^2 vs Error percentage of N=4

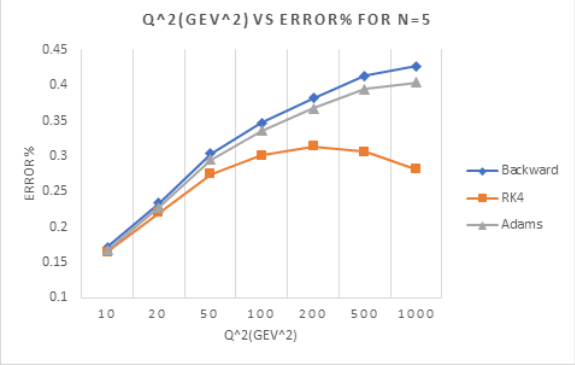

(e) Q^2 vs Error percentage of N=5

Figure 5.3: Q^2 Vs Error of all Methods at Each Number of Steps

5.4 Q^2 Vs Time of all Methods at Each Number of Steps

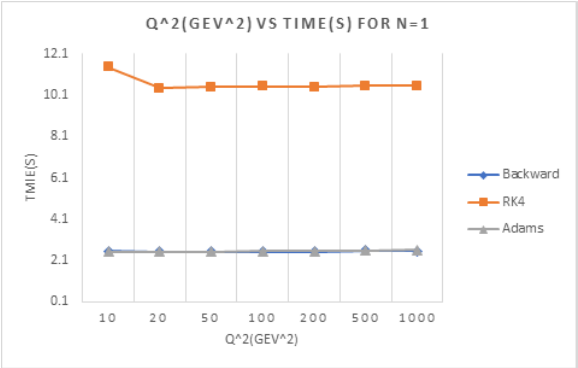

(a) Q^2 vs Time(s) of N=1

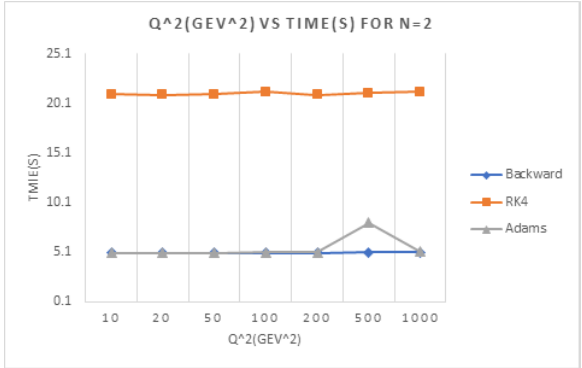

(b) Q^2 vs Time(s) of N=2

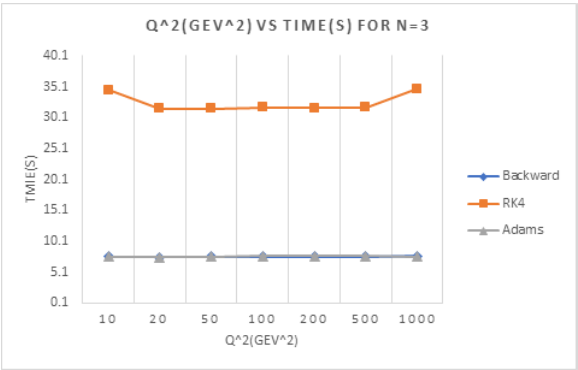

(c) Q^2 vs Time(s) of N=3

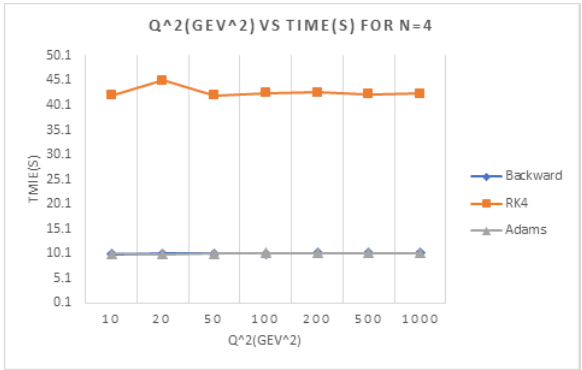

(d) Q^2 vs Time(s) of N=4

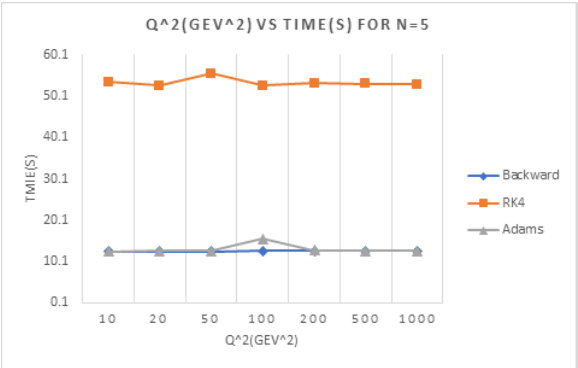

(e) Q^2 vs Time(s) of N=5

Figure 5.4: Q^2 Vs Time of all Methods at Each Number of Steps

5.5 Number of Steps Vs Error of all Q^2 of Each Method

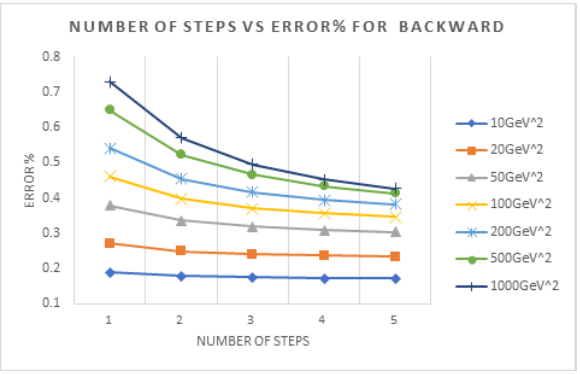

(a) N vs Error percentage of Backward

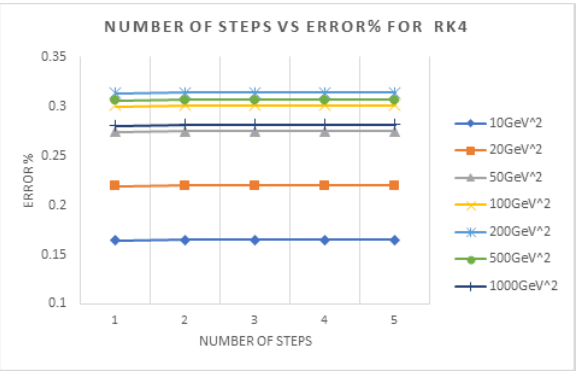

(b) N vs Error percentage of RK4

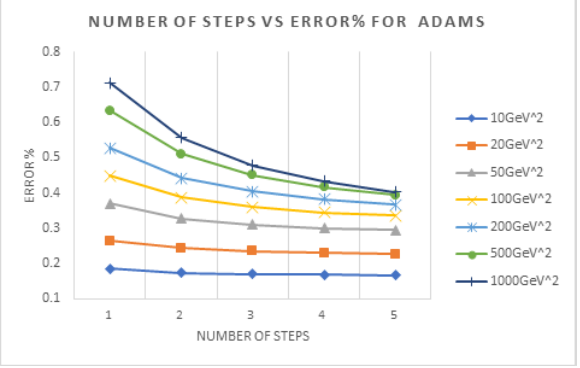

(c) N vs Error percentage of Adams

Figure 5.5: Number of Steps Vs Error of all Q^2 of Each Method

5.6 Number of Steps Vs Time of all Q^2 of Each Method

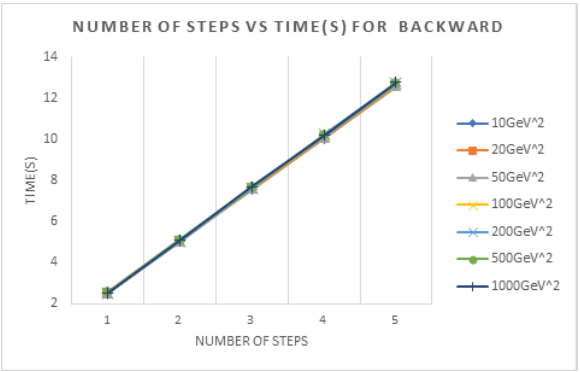

(a) N vs Time(s) of Backward

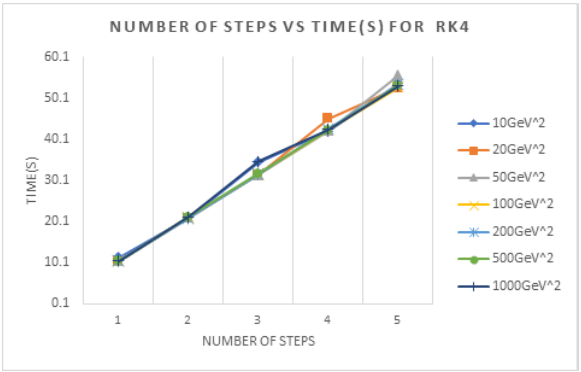

(b) N vs Time(s) of RK4

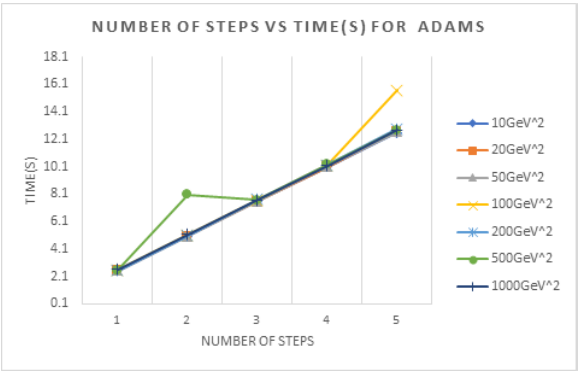

(c) N vs Time(s) of Adams

Figure 5.6: Number of Steps Vs Time of all Q^2 of Each Method

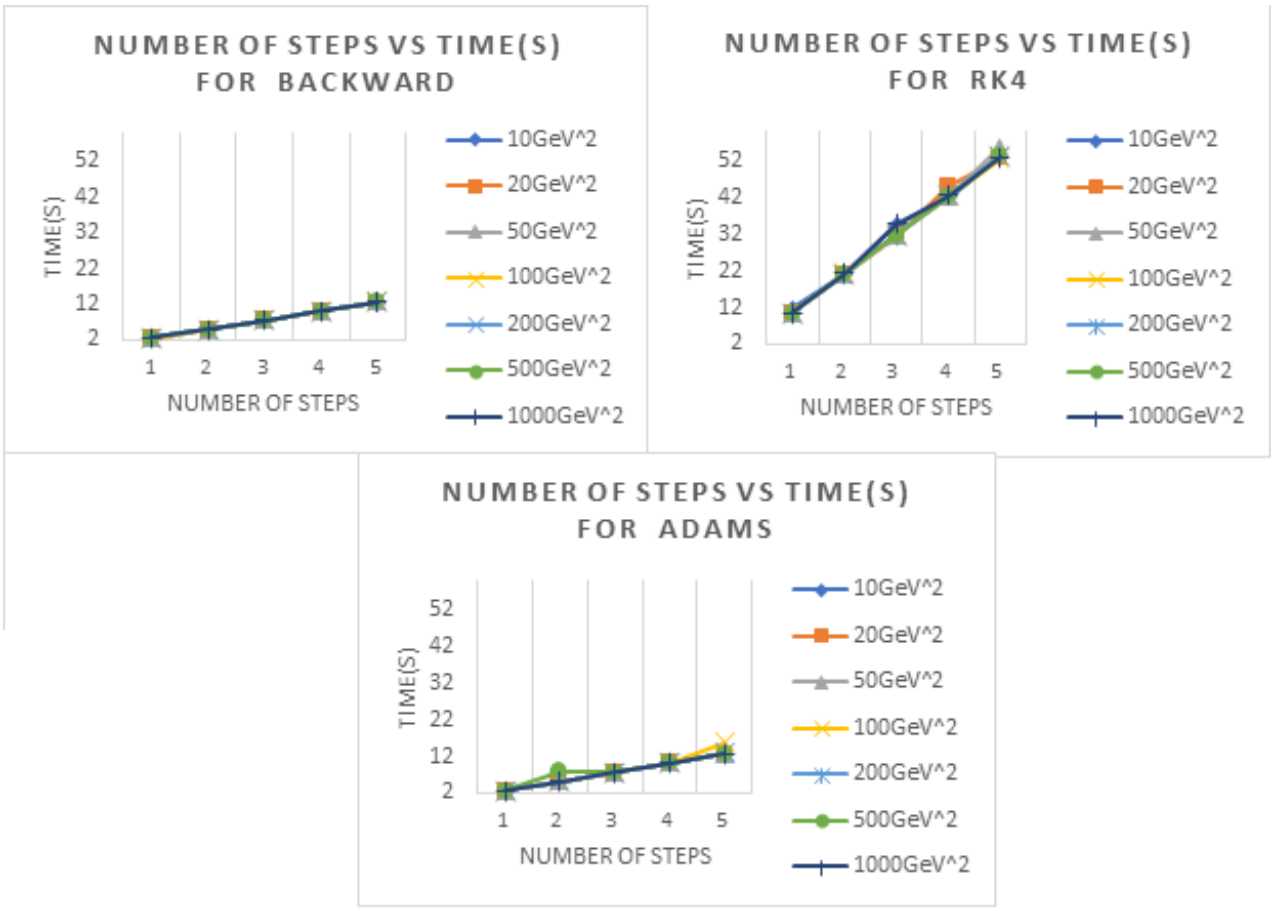

Figure 5.7: N vs Time(s) of All methods

5.7 DGLAP Evolution Limit using the GPD Evolution Equation

The Non-singlet case was used as a checkpoint in this work. As remember in the Chapter1, The DGLAP equation of PDF is

$$\frac{dF^{NS}(x,Q^2)}{dlnQ^2} = C_F\frac{\alpha_s}{2\pi}\Bigg\{\int_x^1 \frac{dz}{1-z}\Big[(1+z^2)F^{NS}\big(\frac{x}{z},Q^2\big) - 2F^{NS}\big(x,Q^2\big)\Big] + \Big[\frac{3}{2} + 2ln(1-x)\Big]F^{NS}\big(x,Q^2\big)\Bigg\} \tag{5.1}$$

And the evolution equation for GPD is

$$\frac{\partial F^{NS}(x,\zeta,Q^2)}{\partial lnQ^2} = C_F\frac{\alpha_s}{2\pi}\Bigg\{\int_x^1 \frac{dz}{1-z}\Big[(1+zz')F^{NS}\big(\frac{x}{z},Q^2\big) - (1+\frac{z'}{z})F^{NS}\big(x,Q^2\big)\Big] + \Big[\frac{3}{2} + ln\frac{(1-x)^2}{1-\zeta}\Big]F^{NS}\big(x,Q^2\big)\Bigg\} \tag{5.2}$$

When $\zeta = 0$, the GPD evolution equation will become the DGLAP equation.

Therefore, another checklist is compare the GPD evolution equation and DGLAP equation in the case of $\zeta = 0$. There should be the same result and sum rules.

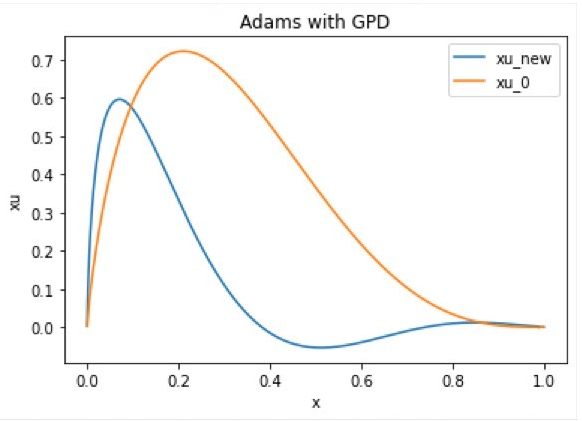

(a) GPD evolution using Adams method

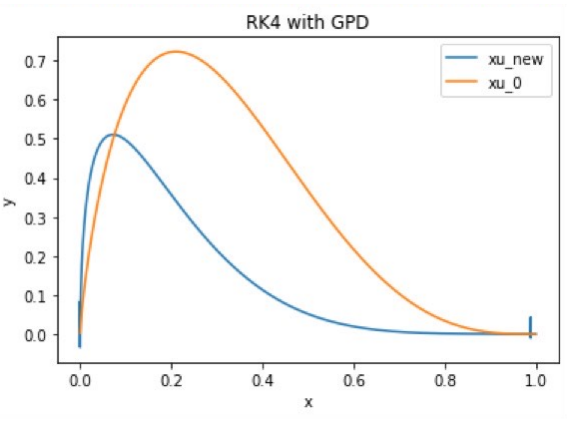

(b) GPD evolution using RK4

```
Total number of u quark before the loop is  1.9959793330526983
Total number of u quark of  0 th loop is  2.005013923233494
Total number of u quark of  1 th loop is  2.00903697074111
The time of execution of Adams is : 10.123729705810547  sec
```

(c) Total u quark and time execution of the GPD evolution using Adams

```
Total number of u quark before the loop is  1.9959793330526983
Total number of u quark of  0 th loop is  2.00200314692317
Total number of u quark of  1 th loop is  1.9989982662995833
The time of execution of RK4 is : 26.301563262939453  sec
```

(d) Total u quark and time execution of the GPD evolution using RK4

Figure 5.8: GPD evolution with Adams and RK4

Chapter 6

Discussion and Conclusions

There are several topics which are discussed and summarized here.

Firstly, I have to clarify that the percentage error which is mentioned in Chapter 4, is the error of every final total number of up quark compare with the initial total number of up quark.

The reason behind this error is the xPDFs only can be retrieved by a fitting process. There are no analytic xPDFs for any energy level except the xPDFs from experiment.

6.1 Number of Steps Vs Error of all Methods at Each Energy Level

The results show the interesting convergence of a decreasing of errors using Adams and Backward methods. They trend to approach the limiting precision of RK4 if the number of steps is increasing. While, the precision of the RK4 always the same even if the number of steps are increased. Moreover, the precision of Adams and Backward are closer at the higher energy scale.

6.2 Number of Steps Vs Time of all Methods at Each Energy Level

The results are as I expect to be. Let compare the Adams and RK4 method

Adams Method :

$$y_{n+1} = y_n + h[f(x_n, y_n) + \frac{1}{2}(f(x,y)_n - f(x,y)_{n-1}) + \frac{5}{12}(f(x,y)_n - 2f(x,y)_{n-1} + f(x,y)_{n-2}) + \frac{3}{8}(f(x,y)_n - 3f(x,y)_{n-1} + 3f(x,y)_{n-2} - f(x,y)_{n-3})] \tag{6.1}$$

RK4 Method :

$$\begin{aligned} y_{n+1} &= y_n + \frac{h}{6}(k_1 + 2k_2 + 2k_3 + k_4) \\ t_{n+1} &- t_n + h \\ k_1 &= f(t_n, y_n) \\ k_2 &= f(t_n + 0.5h, y_n + 0.5hk_1) \\ k_3 &= f(t_n + 0.5h, y_n + 0.5hk_2) \\ k_4 &= f(t_n + h, y_n + hk_3) \end{aligned} \tag{6.2}$$

According to the DGLAP equation, there is a derivative on the left-hand side and an integral of the right-hand side. To solve the equation, the numerical calculation of an integration use a loop to get the array of a derivative.

The k_1, k_2, k_3, k_4 are 4 different loops of integration whereas there is only 1 array of the derivative calling here for the Adams method. The Adams method will pick 4 elements inside the Adams' array. That means the loop of integrations occur 1 time

for the Adams method and 4 times for the RK4 method.

With the same reason, look closely to the results in the chapter 5.2, the time consumption of the RK4 always about 4 times of Adams method.

6.3 Q^2 Vs Error of all Methods at Each Number of Steps

From the data analysis, the behavior of the precision with energy level of RK4 look quadratic.

While, the behavior of Adams and Backward look like a linear at N=1,2,3. Fortunately, I do increase the number of steps to N=4,5. The results of Adams and Backward tend to be a quadratic as well.

We believe that the precision of Adams and Backward will be more precise at the higher number of step. The increasing of a number of steps still show the significant difference of Adams and Backwards.

6.4 Q^2 Vs Time of all Methods at Each Number of Steps

The results of section 5.4 clearly show that the consumption time of RK4 is about 4 times of the time consumed of Adams and Backward methods.

I believe the reason of inflating of time(s) is the discretization of a computer clock(Hz).

6.5 Number of Steps Vs Error of all Q^2 of Each Method

The reults of RK4 method show that the RK4 is a N-independence. In contrary, Adams and Backward methods is a N-dependence.

That means the precision of RK4 is limited, but the precision of Adams and Backward can be improved if the number of steps is increased.

6.6 Number of Steps Vs Time of all Q^2 of Each Method

The comparison of a time consuming with a number of steps show the increasing of time belong with a number of steps linearly.
While the results are plotted with the same scale, the prominent point is the higher rate of time per N of RK4 compared to the Adams and Backward methods.

6.7 Overall Conclusion

All results of the variation of a number of steps and the final energy level are explored to determine the possibility of a precision and time improvement for the DGLAP evolution.

The combination of the execution time vs. the number of steps, the number of steps vs error, and the energy level vs error could lead to an optimization of Adams and

Backward method to further increase the efficiency of the evolution program.

6.8 DGLAP Evolution Limit using the GPD Evolution Equation

As a result, the GPD evolution still conserve total u quark for the NS case as we expected.

This is a good checkpoint as this program will be developed to be a fully GPD evolution in the future.

Appendices

Appendix A

The Plus function

The plus function[Field and Pines 1995] are well behaved distribution when convoluted with a smooth function that vanish sufficiently, rapidly as $x \to 1$. The important property is

$$\int_0^1 dx(F(x))_+ = 0 \tag{A.1}$$

and are defined mathematically by

$$(F(x))_+ \equiv \lim_{\beta \to 0} \left\{ F(x)\theta(1-x-\beta) - \delta(1-x-\beta) \int_0^{1-\beta} F(y)dy \right\} \tag{A.2}$$

where

$$\theta(y) = 0, y \leq 0 \tag{A.3}$$

$$\theta(y) = 1, y > 0 \tag{A.4}$$

The main plus function is

$$\frac{1}{(1-x)_+} \equiv \lim_{\beta \to 0} \left\{ \frac{1}{1-x}\theta(1-x-\beta) + log(\beta)\delta(1-x-\beta) \right\} \tag{A.5}$$

When the plus function convoluted with a well behaved function G(y), the general formula is

$$\int_x^1 \frac{dy}{y}\frac{G(z/y)}{(1-y)_+} = G(z)log(1-z) + \int_x^1 \frac{dy}{y}\frac{G(z/y) - yG(z)}{1-y} \tag{A.6}$$

Bibliography

Rosenbluth, M. N. (1950). "High Energy Elastic Scattering of Electrons on Protons". In: *Phys. Rev.* 79, pp. 615–619. DOI: 10.1103/PhysRev.79.615.

Hofstadter, R. and R.W. McAllister (1955). "Electron Scattering From the Proton". In: *Phys. Rev.* 98, pp. 217–218. DOI: 10.1103/PhysRev.98.217.

Brodsky, Stanley J., Francis E. Close, and J.F. Gunion (1973). "A GAUGE - INVARIANT SCALING MODEL OF CURRENT INTERACTIONS WITH REGGE BEHAVIOR AND FINITE FIXED POLE SUM RULES". In: *Phys. Rev. D* 8, p. 3678. DOI: 10.1103/PhysRevD.8.3678.

Roberts, R. G. (1990). *The Structure of the Proton: Deep Inelastic Scattering*. Cambridge Monographs on Mathematical Physics. Cambridge University Press. DOI: 10.1017/CBO9780511564062.

Field, R.D. and D. Pines (1995). *Applications Of Perturbative Qcd*. Avalon Publishing. ISBN: 9780201483628. URL: https://books.google.com/books?id=2eWnAAAACAAJ.

Golec-Biernat, Krzysztof J. and Alan D. Martin (1999). "Off diagonal parton distributions and their evolution". In: *Phys. Rev. D* 59, p. 014029. DOI: 10.1103/PhysRevD.59.014029. arXiv: hep-ph/9807497.

Burkardt, Matthias (2000). "Impact parameter dependent parton distributions and off forward parton distributions for zeta —> 0". In: *Phys. Rev. D* 62. [Erratum: Phys.Rev.D 66, 119903 (2002)], p. 071503. DOI: 10.1103/PhysRevD.62.071503. arXiv: hep-ph/0005108.

Musatov, I.V. and A.V. Radyushkin (2000). "Evolution and models for skewed parton distributions". In: *Phys. Rev. D* 61, p. 074027. DOI: 10.1103/PhysRevD.61.074027. arXiv: hep-ph/9905376.

Gao, Hai-yan (2003). "Nucleon electromagnetic form-factors". In: *Int. J. Mod. Phys.* E12. [Erratum: Int. J. Mod. Phys.E12,567(2003)], pp. 1–40. DOI: 10.1142/S021830130300117X. arXiv: nucl-ex/0301002 [nucl-ex].

Polyakov, M.V. (2003). "Generalized parton distributions and strong forces inside nucleons and nuclei". In: *Phys. Lett. B* 555, pp. 57–62. DOI: 10.1016/S0370-2693(03)00036-4. arXiv: hep-ph/0210165.

Gorringe, Tim and Harold W. Fearing (2004). "Induced Pseudoscalar Coupling of the Proton Weak Interaction". In: *Rev. Mod. Phys.* 76, pp. 31–91. DOI: 10.1103/RevModPhys.76.31. arXiv: nucl-th/0206039.

Hyde, Charles Earl and Kees de Jager (2004). "Electromagnetic form factors of the nucleon and Compton scattering". In: *Ann. Rev. Nucl. Part. Sci.* 54, pp. 217–267. DOI: 10.1146/annurev.nucl.53.041002.110443. arXiv: nucl-ex/0507001 [nucl-ex].

Ahmad, Saeed et al. (2007). "Generalized Parton Distributions from Hadronic Observables: Zero Skewness". In: *Phys. Rev. D* 75, p. 094003. DOI: 10.1103/PhysRevD.75.094003. arXiv: hep-ph/0611046.

Schindler, M.R. and S. Scherer (2007). "Nucleon Form Factors of the Isovector Axial-Vector Current: Situation of Experiments and Theory". In: *Eur. Phys. J. A* 32.4, pp. 429–433. DOI: 10.1140/epja/i2006-10403-3. arXiv: hep-ph/0608325.

Schienbein, Ingo et al. (2008). "A Review of Target Mass Corrections". In: *J. Phys.* G35, p. 053101. DOI: 10.1088/0954-3899/35/5/053101. arXiv: 0709.1775 [hep-ph].

Ahmad, Saeed et al. (2009). "Generalized Parton Distributions from Hadronic Observables: Non-Zero Skewness". In: *Eur. Phys. J. C* 63, pp. 407–421. DOI: 10.1140/epjc/s10052-009-1073-4. arXiv: 0708.0268 [hep-ph].

Arrington, John, Kees de Jager, and Charles F. Perdrisat (2011). "Nucleon Form Factors: A Jefferson Lab Perspective". In: *J. Phys. Conf. Ser.* 299, p. 012002. DOI: 10.1088/1742-6596/299/1/012002. arXiv: 1102.2463 [nucl-ex].

Kumericki, Kresimir et al. (May 2011). "Accessing GPDs from Experiment — Potential of A High-Luminosity EIC —". In: arXiv: 1105.0899 [hep-ph].

Radyushkin, A. V. (2013). "Topics in theory of generalized parton distributions". In: *Phys. Part. Nucl.* 44, pp. 469–489. DOI: 10.1134/S1063779613030131.

Braun, Vladimir M. et al. (2014). "Deeply Virtual Compton Scattering to the twist-four accuracy: Impact of finite-t and target mass corrections". In: *Phys. Rev.* D89.7, p. 074022. DOI: 10.1103/PhysRevD.89.074022. arXiv: 1401.7621 [hep-ph].

Kumerički, Krešimir and Dieter Müller (2016). "Description and interpretation of DVCS measurements". In: *EPJ Web Conf.* 112, p. 01012. DOI: 10.1051/epjconf/201611201012. arXiv: 1512.09014 [hep-ph].

Afanasev, A. et al. (2017). "Two-photon exchange in elastic electron–proton scattering". In: *Prog. Part. Nucl. Phys.* 95, pp. 245–278. DOI: 10.1016/j.ppnp.2017.03.004. arXiv: 1703.03874 [nucl-ex].

Defurne, M. et al. (2017). "A glimpse of gluons through deeply virtual compton scattering on the proton". In: *Nature Commun.* 8.1, p. 1408. DOI: 10.1038/s41467-017-01819-3. arXiv: 1703.09442 [hep-ex].

Defurne, Maxim (2017). *Results from Hall A on π^0 and photon electroproduction.* URL: http://www.int.washington.edu/talks/WorkShops/int_17_3/People/Defurne_M/Defurne.pdf. (accessed: 01.09.2016).

Georges, Frédéric (2018). "Deeply virtual Compton scattering at Jefferson Lab". PhD thesis. Institut de Physique Nucléaire d'Orsay, France.

Čuić, Marija, Krešimir Kumerički, and Andreas Schäfer (2020). "Separation of Quark Flavors Using Deeply Virtual Compton Scattering Data". In: *Phys. Rev. Lett.* 125.23, p. 232005. DOI: 10.1103/PhysRevLett.125.232005. arXiv: 2007.00029 [hep-ph].

Kriesten, Brandon, Simonetta Liuti, et al. (2020). "Extraction of Generalized Parton Distribution Observables from Deeply Virtual Electron Proton Scattering Experiments". In: *Phys. Rev. D* 101.5, p. 054021. DOI: 10.1103/PhysRevD.101.054021. arXiv: 1903.05742 [hep-ph].

Bogasz, Alex (2021). *https://www.jlab.org/accelerator-seminar-alex-bogacz-remote*. URL: https://www.jlab.org/accelerator-seminar-alex-bogacz-remote.

Dlamini, M. et al. (2021). "Deep Exclusive Electroproduction of $\pi 0$ at High Q2 in the Quark Valence Regime". In: *Phys. Rev. Lett.* 127.15, p. 152301. DOI: 10.1103/PhysRevLett.127.152301. arXiv: 2011.11125 [hep-ex].

Grigsby, Jake et al. (2021). "Deep learning analysis of deeply virtual exclusive photoproduction". In: *Phys. Rev. D* 104.1, p. 016001. DOI: 10.1103/PhysRevD.104.016001. arXiv: 2012.04801 [hep-ph].

Almaeen, Manal et al. (July 2022). "Benchmarks for a Global Extraction of Information from Deeply Virtual Exclusive Scattering". In: arXiv: 2207.10766 [hep-ph].

Georges, F. et al. (2022). "Deeply Virtual Compton Scattering Cross Section at High Bjorken xB". In: *Phys. Rev. Lett.* 128.25, p. 252002. DOI: 10.1103/PhysRevLett.128.252002. arXiv: 2201.03714 [hep-ph].

Kriesten, Brandon and Simonetta Liuti (2022). "Theory of deeply virtual Compton scattering off the unpolarized proton". In: *Phys. Rev. D* 105.1, p. 016015. DOI: 10.1103/PhysRevD.105.016015. arXiv: 2004.08890 [hep-ph].

Shiells, Kyle, Yuxun Guo, and Xiangdong Ji (2022). "On extraction of twist-two Compton form factors from DVCS observables through harmonic analysis". In: *JHEP* 08, p. 048. DOI: 10.1007/JHEP08(2022)048. arXiv: 2112.15144 [hep-ph].